



Published in final edited form as:

*Nat Chem Biol.* 2021 July ; 17(7): 784–793. doi:10.1038/s41589-021-00815-5.

## Small molecule inhibitors targeting Polycomb Repressive Complex 1 RING domain

Shirish Shukla<sup>1,4</sup>, Weijiang Ying<sup>1,4</sup>, Felicia Gray<sup>1,4</sup>, Yiwu Yao<sup>1,4</sup>, Miranda L. Simes<sup>1,4</sup>, Qingjie Zhao<sup>1</sup>, Hongzhi Miao<sup>1</sup>, Hyo Je Cho<sup>1</sup>, Paula González-Alonso<sup>1</sup>, Alyssa Winkler<sup>1</sup>, George Lund<sup>1</sup>, Trupta Purohit<sup>1</sup>, EunGi Kim<sup>1</sup>, Xiaotian Zhang<sup>1</sup>, Joshua M. Ray<sup>1</sup>, Shihan He<sup>1</sup>, Caroline Nikolaidis<sup>1</sup>, Juliano Ndoj<sup>1</sup>, Jingya Wang<sup>1,6</sup>, Łukasz Jaremko<sup>3</sup>, Mariusz Jaremko<sup>3</sup>, Russell J.H. Ryan<sup>1</sup>, Monica L. Guzman<sup>2</sup>, Jolanta Grembecka<sup>1,5,\*</sup>, Tomasz Cierpicki<sup>1,5,\*</sup>

<sup>1</sup>Department of Pathology, University of Michigan, Ann Arbor, MI, USA

<sup>2</sup>Division of Hematology and Medical Oncology, Leukemia Program, Weill Cornell Medicine/New York-Presbyterian Hospital, New York, NY, USA.

<sup>3</sup>King Abdullah University of Science and Technology (KAUST), Biological and Environmental Science and Engineering (BESE), Thuwal, Saudi Arabia.

<sup>4</sup>these authors equally contributed to this work

<sup>5</sup>these authors jointly supervised this work

<sup>6</sup>Present address: MedImmune, LLC, Gaithersburg, MD, USA

### Abstract

Polycomb repressive complex 1 (PRC1) is an essential chromatin modifying complex that monoubiquitinates histone H2A and is involved in maintaining the repressed chromatin state. Emerging evidence suggests PRC1 activity in various cancers, rationalizing the need for small molecule inhibitors with a well-defined mechanism of action. Here, we describe the development of compounds that directly bind to RING1B-BMI1, the heterodimeric complex constituting the E3 ligase activity of PRC1. These compounds block the association of RING1B-BMI1 with chromatin and inhibit H2A ubiquitination. Structural studies demonstrate that these inhibitors bind to RING1B by inducing the formation of a hydrophobic pocket in the RING domain. Our PRC1 inhibitor, RB-3, decreases the global level of H2A ubiquitination and induces differentiation in leukemia cell lines and primary AML samples. In summary, we demonstrate that targeting the PRC1 RING domain with small molecules is feasible, and RB-3 represents a valuable chemical tool to study PRC1 biology.

---

Users may view, print, copy, and download text and data-mine the content in such documents, for the purposes of academic research, subject always to the full Conditions of use: [http://www.nature.com/authors/editorial\\_policies/license.html#terms](http://www.nature.com/authors/editorial_policies/license.html#terms)

\*corresponding authors: tomaszc@umich.edu; jolantag@umich.edu.

Author contributions

TC and JG were responsible for initiating and supervising the project. SS, FG, HM, PGA, MS, AW, TP, SH, CN, JN, JW, XZ, JMR, EK performed screening, testing biochemical activity, cell based studies and animal studies; HJC, FG, GL, ŁJ, MJ carried out structural biology studies; WY, YY, QZ synthesized compounds; MLG, RJHR provided reagents and advised the study. All authors contributed to data analysis and writing the manuscript.

Competing interests

WY, YY, FG, QZ, JG, TC are co-inventors on patent application for PRC1 inhibitors.

Polycomb repressive complex 1 (PRC1) and 2 (PRC2) are essential epigenetic regulators involved in recognition and posttranslational modifications of histone proteins and are implicated in establishing and maintaining the repressive chromatin state<sup>1,2</sup>. The core of PRC1 consists of heterodimeric complexes involving RING1A/B and one of the six PCGF1–6 paralogs, thereby resulting in six distinct complexes PRC1.1 to PRC1.6<sup>2–5</sup>. The major biochemical activity of PRC1 is monoubiquitination of Lys119 on histone H2A (H2Aub) that is generally associated with transcriptional repression<sup>6–8</sup>. Such an activity is conferred by the canonical PRC1 complexes PRC1.2 (with PCGF2/MEL18) and PRC1.4 (with PCGF4/BMI1). The heterodimeric complex composed of the RING domains of RING1B and BMI1 constitutes the core of the canonical PRC1 and the minimal E3 ligase unit sufficient for H2A ubiquitination *in vitro*<sup>4,6,9</sup>. The function of non-canonical complexes contributes to the recruitment of PRC1 to chromatin, and while PRC1.1 is associated with repressed chromatin and formation of polycomb domains<sup>10–12</sup>, PRC1.3 and PRC1.6 bind to actively transcribed genes<sup>5</sup>.

Leukemic stem cells (LSCs) or leukemia-initiating cells (LICs) represent a rare population of cells that are capable of self-renewal, proliferation and differentiation into malignant blasts<sup>13,14</sup>. The self-renewal and differentiation capacity of stem cells, including LSCs, is dependent on the activity of polycomb group proteins (PcG)<sup>15–18</sup>. BMI1 is a key component of canonical PRC1, which determines proliferative and self-renewal capacity of normal and leukemic stem cells<sup>17</sup>, and *BMI1* knockdown impairs LSC self-renewal and induces apoptosis in AML stem cells<sup>19</sup>. Activity of RING1A/B is also essential for the maintenance of AML stem cells<sup>18</sup> and leukemogenesis<sup>20</sup>. Therefore, blocking PRC1 activity with small molecules could lead to the eradication of leukemic stem cells, providing a potential therapeutic approach to improve survival outcome in AML patients.

To date, several attempts approached targeting PRC1 activity with small molecules. For example, PTC-209 induces BMI1 degradation and reduces H2Aub levels, but its mechanism of action and selectivity have not been fully elucidated<sup>14</sup>. Other compounds described to reduce the activity of PRC1 include PRT4165<sup>21</sup> and GW-516<sup>22</sup>; however, these compounds have not been shown to directly bind to PRC1, and their mechanism of action also remains unknown. In this work, we employed fragment-based ligand discovery to develop the first-in-class small molecules that directly bind to the RING1B and RING1A proteins and inhibit PRC1 activity through blocking the interaction of the E3 ligase core of the PRC1 complex with nucleosomes. Our lead compound, RB-3, decreases global level of H2Aub and induces differentiation in leukemia cells and primary AML samples, therefore representing an attractive and unique agent for studying PRC1 biology. This work demonstrates that directly targeting H2A ubiquitination activity of PRC1 with small molecules is feasible and may lead to the development of pharmaceutical agents for leukemia and possibly other cancers.

## Results

### Development of PRC1 inhibitors using fragment screening

To develop inhibitors of PRC1 activity, we aimed to identify small molecules capable of directly targeting the heterodimeric E3 ligase composed of RING1B and BMI1, the core components of PRC1. In order to facilitate purification of recombinant protein, we designed

a fusion of the RING1B and BMI1 RING domains (hereafter referenced as RING1B-BMI1f). Recombinant  $^{15}\text{N}$ -labeled RING1B-BMI1f yields high quality NMR spectra, and we used this protein for screening of a fragment library of ~1000 molecules using  $^1\text{H}$ - $^{15}\text{N}$  HSQC experiments. The most potent hit identified was RB-1 (**1**), which weakly binds to RING1B-BMI1f with an estimated 7 mM binding affinity (Fig. 1a, Extended Data Fig. 1a). We then developed a H2A ubiquitination assay and found that RB-1 inhibits E3 ligase activity of RING1B-BMI1f at mM concentrations (Extended Data Fig. 1b). By employing NMR experiments, we assigned chemical shifts of RING1B-BMI1f to map the binding site of the fragment hit, and demonstrated that RB-1 binds to the RING domain of RING1B (Extended Data Fig. 1c). To further validate that RB-1 binds to a site relevant to E3 ligase activity, we mutated K85 in RING1B, a residue in a region that experiences large chemical shift perturbations upon RB-1 binding (Extended Data Fig. 1c). The K85E point mutation significantly abolished H2A ubiquitination activity of RING1B-BMI1f (Extended Data Fig. 1b), emphasizing that RB-1 engages a functionally relevant site on RING1B. Subsequent optimization of RB-1 started from changing the thiophene ring to a more soluble pyrrole, and extensive medicinal chemistry led to the much more potent RB-2 (**2**) (Fig. 1a). Binding of RB-2 to RING1B-BMI1f was validated in NMR HSQC experiments, demonstrating substantial chemical shift perturbations and suggesting structural perturbations in RING1B (Fig. 1b). To determine binding affinity of RB-2 towards RING1B-BMI1f we performed NMR titration, which resulted in  $K_D = 11.5 \mu\text{M}$  (Fig. 1c). We further tested activity of RB-2 in H2A ubiquitination assays and found that it inhibits E3 ligase activity of RING1B-BMI1f with  $\text{IC}_{50} \sim 12 \mu\text{M}$  (Fig. 1d), which is in concordance with its binding affinity.

### PRC1 inhibitor changes conformation of the RING domain

Analysis of the crystal structure of RING1B-BMI1 reveals a lack of any pockets for small molecule binding. To understand the binding mode of RB-2 we determined the crystal structures of both, free RING1B-BMI1f (Extended Data Fig. 2a, Supplementary Table 1) and RING1B-BMI1f co-crystallized with RB-2, (Fig. 1e, Extended Data Fig. 2b, Supplementary Table 1). The crystal structure of free RING1B-BMI1f is very similar to the previously reported heterodimeric RING1B-BMI1 structures (backbone RMSD = 0.26 Å, Extended Data Fig. 2a)<sup>6,23</sup>. In the case of RING1B-BMI1f co-crystallized with the inhibitor, we did not observe the electron density for RB-2, likely due to relatively low resolution (3.1 Å) (Extended Data Fig. 2b). However, in this structure we observed significant conformational changes in the RING domain, particularly involving RING1B residues K93 to S99 and disruption of the  $3_{10}$  helix with the shift of K97 C $\alpha$  by 4.3 Å (Fig. 1e). This conformational change exposed a hydrophobic pocket including the side chains of I77, L80, L100 in the RING domain (Fig. 1f, Extended Data Fig. 2c), and no such pocket is present in the closed conformation observed for free protein (Fig. 1g). These structural perturbations are consistent with the extensive chemical shift perturbations in RING1B upon binding of RB-2 (Extended Data Fig. 2d).

To understand the molecular details of RB-2 binding to RING1B, we employed NMR and expressed  $^2\text{H}$ ,  $^{13}\text{C}$ ,  $^{15}\text{N}$  labeled RING1B-BMI1f with  $^1\text{H}$  methyl labeled Ile, Val and Leu. Following the chemical shift assignment, we recorded 3D  $^{13}\text{C}$ -separated HSQC-NOESY for free RING1B-BMI1f and RING1B-BMI1f in complex with RB-2 and observed multiple

intermolecular NOEs between side chains of aliphatic residues in RING1B and RB-2 (Extended Data Fig. 2e). To determine a structural model of RING1B-BMI1f with bound inhibitor, we employed the 3.1 Å resolution crystal structure in an open conformation and intermolecular distances from NMR. Modeling of the complex with RB-2 based on the hybrid approach employing X-ray crystallography and NMR data was performed using the HADDOCK2.4 program (Fig. 1h, Extended Data Fig. 2f,g, Supplementary Table 2)<sup>24</sup>. We found that RB-2 occupies an elongated hydrophobic pocket generated upon conformational change in RING1B, with the main interface involving the side chains of M62, I76, I77, L80, L94, and L100 (Fig. 1h,i). The surrounding area of the binding site is positively charged due to the presence of R81, K85, K97, and R98, which justifies the need for the carboxyl group in RB-2 (Fig. 1i). Importantly, such a binding mode correlates very well with the chemical shift perturbations observed upon binding of RB-2 (Fig. 1h). To further validate the binding mode and the importance of hydrophobic contacts, we mutated the entirely buried L94 to Ala and found that it nearly abolished the interaction of RB-2 with RING1B-BMI1f without disrupting the protein structure as judged from NMR spectra (Extended Data Fig. 2h).

### Development of improved PRC1 inhibitor

By employing the structural model of RING1B-BMI1f-RB-2, we designed a more potent compound, RB-3 (**3**), by replacing ethyl with isopropyl and chloro-phenyl with chloro-indole to increase hydrophobic contacts with RING1B. RB-3 binds to RING1B-BMI1f with  $K_D = 2.8 \pm 0.45 \mu\text{M}$  (Fig. 2a,b) and induces very extensive chemical shift perturbations in RING1B, including amide protons and methyl groups (Fig. 2c, Extended Data Fig. 3a). RB-3 inhibits H2A ubiquitination with  $IC_{50} = 1.6 \mu\text{M}$  and is about 5-fold more potent than RB-2 (Fig. 2d). We also developed a structurally similar and significantly weaker compound, RB-nc (**4**), by introducing a hydroxyethyl substituent to the indole ring (Fig. 2a). RB-nc weakly binds to RING1B-BMI1f ( $K_D = 344 \mu\text{M}$ ) and does not inhibit RING1B-BMI1 activity (Extended Data Fig. 3b,c), and therefore it served as a negative control compound.

The core of all PRC1 complexes requires the presence of one of the two paralogs, RING1B or RING1A<sup>2,3,5</sup>. Sequence comparison of these paralogs indicates high identity with only 8 different amino acids within the RING domains. We employed NMR and found that RB-3 binds to both, RING1A-BMI1f and RING1B-BMI1f, inducing similar concentration-dependent chemical shift perturbations (Extended Data Fig. 3d,e). Furthermore, the inhibitory activity of RB-3 in the H2A ubiquitination assay is very similar for both PRC1 complexes (Extended Data Fig. 3f).

RING1B forms the heterodimeric E3 ligase with one out of six PCGF paralogs<sup>4</sup>, and based on recent work, the most pronounced H2A ubiquitination activity is executed by PRC1.1 and PRC1.2/4 complexes<sup>5</sup>. To test whether RB-3 inhibits the activity of different PRC1 complexes, we expressed heterodimeric RING1B-PCGF1 and RING1B-BMI1 complexes and observed very similar activity of RB-3 *in vitro* (Fig. 2d). Altogether, our data strongly suggest that RB-3 functions as a general PRC1 inhibitor blocking H2A ubiquitination through direct binding to both RING1B and RING1A.

To assess selectivity, we tested RB-3 against other E3 ligases involved in H2A ubiquitination, such as TRIM37<sup>25</sup>, BRCA1-BARD1<sup>26</sup> and RNF168<sup>27</sup>, and found no inhibition of their activity or binding to these proteins in solution (Extended Data Fig. 3g and Supplementary Fig. 1). We further expressed several RING domains of the closest homologs of RING1B, including RNF4, TRAF6, and TRIM31, and found that RB-3 does not bind to these proteins (Supplementary Fig. 1). The selectivity of RB-3 is supported by structural analysis of the most similar RING domains, demonstrating no conserved residues involved in inhibitor binding (Supplementary Fig 2). We also profiled RB-3 in a broad panel of 291 protein kinases and found lack of any significant off-target activity (Supplementary Fig. 3a). In addition, we validated that RB-3 does not show any significant inhibition of epigenetic enzymes, including histone deacetylases and histone methyltransferases (Supplementary Fig. 3b,c). Importantly, RB-3 has no effect on the activity of EZH2, confirming the lack of inhibition of PRC2 (Supplementary Fig. 3c). RB-3 showed no binding to a panel of bromo and chromodomains (Supplementary Fig. 3d) and lacks binding to DNA (Supplementary Fig. 4).

To further validate whether RB-3 selectively binds PRC1 proteins from human cells, we synthesized two biotinylated probes, RB-3-biot (5) and RB-nc-biot (6), representing respectively, active and inactive analogs (Extended Data Fig. 4a). Binding of RB-3-biot but not RB-nc-biot to RING1B-BMI1f was validated by NMR (Extended Data Fig. 4b). We subsequently performed pull-down experiments from HEK293T cells and found that only RB-3-biot can efficiently pull-down endogenous RING1B and BMI1 (Extended Data Fig. 4c). Overall, RB-3 is the first-in-class inhibitor of PRC1 with low micromolar activity and high selectivity, making it suitable for cell-based studies.

### RB-3 blocks binding of RING1B to the nucleosome

Primary activity of RING1B-BMI1 as an E3 ligase is to facilitate the interaction of an E2-ubiquitin conjugate with the nucleosome substrate. Structural studies revealed that the RING domain of RING1B mediates contact with the nucleosome<sup>9</sup>. Interestingly, mapping of the RB-2 and RB-3 binding site indicates that these inhibitors bind at the interface of RING1B that is utilized to associate with the nucleosome (Fig. 2e). Thus, we hypothesized that RB-3 inhibits E3 ligase activity of RING1B-BMI1 via blocking its interaction with nucleosome. To confirm this, we developed an AlphaLisa assay detecting the binding of His-tagged RING1B-BMI1f with biotinylated nucleosomes and found that RB-3 blocks RING1B-BMI1f-nucleosome interaction with  $IC_{50} = 2 \mu M$  (Fig. 2f). We further validated that RB-3 disrupts the RING1B-BMI1f interaction with recombinant nucleosomes in a gel shift assay (Fig. 2g). To assess whether RB-3 is a cell permeable inhibitor that blocks binding of full length RING1B with chromatin in cells, we utilized a NanoBiT protein complementation assay<sup>28</sup>. We co-expressed LgBiT-RING1B and SmBiT-H3.3 in HEK293T cells and observed a strong luminescence signal, reflecting binding of PRC1 containing LgBiT-RING1B to SmBiT-H3.3-labeled nucleosomes in live cells (Supplementary Fig. 5). The RING1B R98A point mutation was shown to strongly reduce binding of the core PRC1 module to nucleosome<sup>9</sup>. Concordantly, the R98A mutation in LgBiT-RING1B significantly decreased the luminescence signal in NanoBit (Supplementary Fig. 5). Treatment of HEK293T cells with RB-3 reduced the luminescence signal in a dose-dependent manner, with a cellular  $IC_{50}$

= 6  $\mu$ M (Fig. 2h). These results demonstrate that RB-3 inhibits RING1B interaction with chromatin in live cells. In contrast, no activity was observed for RB-nc in the NanoBiT assay (Fig. 2h), validating this compound as a negative control for cell-based experiments.

Structural studies of the PRC1-nucleosome complex revealed that RING1B recognizes an acidic patch on the nucleosome core via K97 and R98 side chains (so-called arginine anchor)<sup>9</sup>. Analysis of the crystal structures of free RING1B-BMI1f and RING1B-BMI1f co-crystallized with RB-2 show that our PRC1 inhibitors induce a conformational change that distorts the arginine anchor motif in RING1B, further rationalizing disruption of its binding to the nucleosome (Fig. 2i).

### RB-3 inhibits activity of PRC1 in cancer cells

We then assessed whether RB-3 inhibits the activity of PRC1 in cancer cells. Indeed, treatment of the K562 leukemia cell line with RB-3 resulted in a strong reduction in H2Aub without affecting H2Bub, validating specific inhibition of PRC1 (Extended Data Fig. 5a). Importantly, the protein levels of RING1B and BMI1 were not affected by RB-3 (Extended Data Fig. 5a). A decrease in H2Aub induced by RB-3 was also consistent with the effect observed upon knockdown of RING1B or BMI1 (Extended Data Fig. 5a). We also performed similar experiments in HeLa cells, and treatment with RB-3 as well as silencing of RING1B or BMI1 markedly reduced H2Aub levels (Extended Data Fig. 5b). Furthermore, RB-3, but not RB-nc, decreased global levels of H2Aub in AML cell lines MOLM13 and MV4;11 (Extended Data Fig. 5c,d). Overall, RB-3 broadly inhibits the activity of PRC1 in various cancer cell lines, which is consistent with its activity in biochemical and binding assays.

### RB-3 induces differentiation in TEX leukemia cells

Next, we selected TEX cells, which mimic features of leukemia-initiating cells (LICs)<sup>29,30</sup> to characterize the activity of RB-3. TEX cells are derived from HSPCs transformed with the TLS-ERG oncogene and express high levels of CD34 and low levels of CD38, which serve as LIC markers<sup>29,30</sup>. Treatment of TEX cells with RB-3 led to a marked reduction in H2Aub level at day 4 (Fig. 3a), which was further enhanced upon longer treatment (Extended Data Fig. 6a). Importantly, the level of H2Bub (Fig. 3a, Extended Data Fig. 6a) or global protein ubiquitination were not affected (Extended Data Fig. 6b). We tested viability of TEX cells treated with RB-3 and found moderate and time-dependent growth inhibition (Fig. 3b). Subsequently, we investigated whether reduction of H2Aub level impacts activity of TEX cells. Using flow cytometry, we validated a high level of CD34 and a low level of CD38 markers in DMSO-treated TEX cells and strong reduction of CD34<sup>+</sup> upon treatment with RB-3 (Fig. 3c, Extended Data Fig. 6c). Interestingly, longer treatment of TEX cells with RB-3 resulted in a significant shift from CD34<sup>+</sup>/CD38<sup>low</sup> to CD34<sup>-</sup>/CD38<sup>high</sup> population (Fig. 3c, Extended Data Fig. 6d). The cells treated with RB-3 showed dose-dependent reduction of CD34 from 87% to 26%, while initial low level of CD38<sup>+</sup> cells was increased from 12% to 90%. Altogether, such an effect suggests loss of stem cell features<sup>13,31</sup>. We further characterized RB-3 treated TEX cells and found an increase in the expression of the myeloid marker CD11b, a complete shift from CD86<sup>-</sup> to CD86<sup>+</sup> cells, and a morphology change, all of which are consistent with differentiation of TEX cells (Fig 3d,e,f, Extended

Data Fig 6e,f,g). Importantly, the negative control compound RB-nc did not induce differentiation of TEX cells (Fig 3c,d,e,f, Extended Data Fig 6d,f,g).

### RB-3 reduces H2Aub via disruption of PRC1 binding

To understand the mechanism of RB-3 activity, we performed global gene expression studies in TEX cells treated with RB-3 for 6 and 10 days (Fig. 4a, Supplementary Fig. 6a). Notably, gene-set enrichment analysis revealed changes in the gene expression signatures related to hematopoietic stem cells (HSCs) and LSCs (Fig. 4b,c, Supplementary Fig. 6b,c). For example, we observed strong enrichment for genes down-regulated in LSCs (CD34<sup>+</sup>CD38<sup>-</sup>) (Fig. 4b) which became upregulated upon treatment with RB-3. Conversely, genes upregulated in CD133<sup>+</sup> HSCs became down-regulated upon treatment with RB-3 (Fig. 4c). Analysis of the gene expression data confirmed a dose- and time-dependent downregulation of CD34 and upregulation of CD86 expression upon treatment with RB-3 (Fig. 4d, Extended Data Fig. 7a). In addition, we observed a marked upregulation of the *C/EBPα* transcript and *C/EBPα*-p42 protein level (Fig. 4d,e, Extended Data Fig. 7a). *C/EBPα* is an important tumor suppressor and myeloid differentiation factor frequently disrupted in leukemia<sup>32</sup>. To understand the mechanism of *C/EBPα* upregulation, we performed chromatin immunoprecipitation (ChIP) and found that RB-3 (Fig. 4f), but not RB-nc (Extended Data Fig. 7b), reduced the H2Aub level at the *C/EBPα* promoter. This was accompanied by decreased binding of RING1B to the *C/EBPα* promoter, suggesting that RB-3 reduces occupancy of PRC1 at *C/EBPα* (Fig. 4f). An increased expression of *C/EBPα* also correlates with the elevated H3K4me3 activating mark (Fig. 4f). We also found that RB-3 reduced H2Aub and decreased the binding of RING1B at the promoters of other genes, such as CD34 and CD11b (Extended Data Fig. 7c,d), supporting a mechanism in which RB-3 reduces H2Aub by inhibiting the recruitment of PRC1 to the target genes. These ChIP experiments further validate that RB-3 disrupts PRC1 interaction with chromatin, which is consistent with the data obtained using our NanoBiT assay (Fig. 2h).

We then performed ChIP-seq analysis of TEX cells treated with RB-3 and found compound-induced global reduction in H2Aub levels at gene promoters and gene bodies (Extended Data Fig. 7e). In case of the *C/EBPα* gene, we observed a high level of H2Aub that is uniformly reduced upon treatment with RB-3 (Fig. 4g) and correlates with increased *C/EBPα* expression, consistent with H2Aub as a repressive mark<sup>1</sup>. However, global expression analysis in TEX cells indicates a higher number of genes downregulated rather than upregulated by RB-3 (Fig. 4a), which suggests indirect transcriptional outcomes upon PRC1 inhibition<sup>33,34</sup>. To investigate this further, we performed correlation analysis of ChIP-seq and RNA-seq data for the subsets of the most perturbed genes. Genes most strongly de-repressed by RB-3 show an elevated level of H2Aub, which is then reduced by treatment with RB-3 (Fig. 4h). On the contrary, genes downregulated by RB-3 are neither showing high levels of H2Aub, nor do these levels decrease upon treatment with RB-3 (Fig. 4h). This suggests that RB-3 has the most pronounced effect on genes with high levels of H2Aub, which are repressed by PRC1 in TEX cells. We have also noted that treatment of TEX cells with RB-3 did not upregulate *INK4A-ARF*, an established locus repressed by PRC1<sup>35</sup>. In agreement, introduction of the catalytically inactive RING1B I53S mutant in ES cells also failed to de-repress *INK4A*<sup>7</sup>.

We also tested the activity of PTC209, a small molecule that was reported to reduce BMI1 transcript levels<sup>14</sup>. PTC209 was more cytotoxic to TEX cells than RB-3 (Extended Data Fig. 8a), and treatment with PTC209 resulted in decreased H2Aub, reduced BMI1 level and, unexpectedly, reduced H2A levels (Extended Data Fig. 8b). In contrast to RB-3, treatment with PTC209 had no effect on C/EBP $\alpha$  and CD34 expression, indicating different mechanisms of action (Extended Data Fig. 8c,d). In support, the treatment of CD34<sup>+</sup> AML cells with PTC209 induced apoptosis rather than differentiation<sup>36</sup>.

### RB-3 reduces colony formation in an MLL-ENL model

Next, we assessed the activity of RB-3 in MLL-ENL cells, representing another surrogate for LIC<sup>37</sup>. These cells have been developed by transforming lineage negative cord blood cells with the MLL-ENL oncogene, which have very frequent LSCs and are capable of forming colonies<sup>37</sup>. Treatment of MLL-ENL cells with RB-3 markedly reduced global H2Aub levels, but this was not seen when treated with RB-nc (Fig. 5a). MLL-ENL cells are CD34 negative, and to evaluate the effect of RB-3 on differentiation we assessed C/EBP $\alpha$  expression. Indeed, RB-3 markedly increased the expression and protein level of C/EBP $\alpha$ -p42 (Fig. 5b,c). We also performed colony formation assays to evaluate the activity of RB-3 on self-renewal capacity of MLL-ENL cells. Treatment with RB-3, but not with RB-nc, significantly decreased colony numbers in a dose-dependent manner (Fig. 5d,e) indicating that our PRC1 inhibitor impairs clonogenic potential of these cells.

### RB-3 induces differentiation in human primary leukemia cells

We then tested the activity of RB-3 in four primary CD34<sup>+</sup> AML samples (Supplementary Fig. 7a). Consistent with TEX and MLL-ENL cells, we observed decreased H2Aub levels upon treatment with RB-3 (Fig. 6a). Treatment with RB-3 also reduced colony formation (Fig. 6b) and decreased the level of CD34<sup>+</sup> cells in these primary samples (Fig. 6c,d, Supplementary Fig. 7b). Most notably, RB-3 markedly induced differentiation in the tested primary AML samples. Three out of four samples (samples #1, #2, #4) had significantly increased CD11b (Fig. 6e,f) and two samples (samples #1, #4) showed elevated C/EBP $\alpha$  protein levels (Fig. 6g). Strikingly, the effects observed upon treatment of sample #4 revealed very similar changes as in TEX cells, namely a decrease in CD34<sup>+</sup>, increase in CD11b, induction of C/EBP $\alpha$  expression, and shift from negative to 97% CD86<sup>+</sup> cells (Fig. 6c,e,g,h). AML sample #3, which had the highest population of CD34<sup>+</sup> cells, did not show an increase in CD11b; however, morphology changes upon treatment with RB-3 are also consistent with differentiation (Fig. 6i). We also treated normal human CD34<sup>+</sup> cord blood cells with RB-3 and did not observe any significant effects on colony number, types of colonies or change in the population of CD34<sup>+</sup> cells (Extended Data Fig. 9), supporting limited toxicity of this compound on normal hematopoietic progenitor cells. Overall, inhibition of PRC1 with RB-3 in primary AML samples leads to various levels of differentiation through different mechanisms. Furthermore, the pronounced activity of RB-3 in AML cells when compared to normal CD34<sup>+</sup> cells suggests that inhibition of PRC1 may offer an approach to induce differentiation of leukemia cells.

## Discussion

Histone ubiquitination is an essential process in regulating gene transcription and is frequently altered in cancer<sup>38</sup>. PRC1 is a major complex that introduces ubiquitination of K119 on H2A, and its activity is needed for maintenance of hematopoietic stem cells<sup>39</sup>. Accumulating evidence also implicates PRC1 in regulation of AML stem cells and leukemogenesis<sup>17–19</sup>, establishing PRC1 as an attractive target for development of new therapeutics. In this work, we employed a fragment-based ligand discovery technique and developed RB-3, a first-in-class small molecule that directly binds to the RING domain of RING1B and RING1A and inhibits PRC1 H2A ubiquitination activity. Mechanistically, RB-3 blocks the interaction of RING1B-BMI1 with the nucleosome *in vitro* and association of PRC1 with chromatin in cells, resulting in the inhibition of H2A ubiquitination. RB-3 represents the protein-nucleosome interaction inhibitor with a cellular IC<sub>50</sub> ~ 6 μM and a well validated mechanism of action. We evaluated activity of RB-3 in two cell lines mimicking features of LICs and primary AML samples and found that it induces cellular differentiation, suggesting that inhibiting PRC1 might represent a strategy to target LSCs. Intriguingly, RING1B might play an E3 ligase role outside of PRC1 complex, e.g. facilitating degradation of topoisomerase 2<sup>21</sup> or p53<sup>40</sup>, and further studies might explore RB-3 activity in such models.

A family of RING E3 ligases represents appealing targets for inhibitor development<sup>41</sup>. To date, one of the most successful examples of RING E3 ligase inhibitors involves small molecules targeting the activity of MDM2 via blocking the interaction with p53<sup>42</sup>. However, development of small molecules directly binding to RING domains is challenging due to compact sizes of RING domains and the lack of well-defined pockets. We tackled this problem by performing NMR-based fragment screening that yielded a weakly binding compound RB-1 that we subsequently improved over 2500-fold and developed the low micromolar inhibitor RB-3. RB-3 binds to RING1B by inducing conformational changes in the RING domain, resulting in the formation of a well-defined hydrophobic pocket. This example provides precedence for the feasibility of directly targeting RING domains with small molecules. Notably, novel E3 ligase ligands are also in high demand for development of small molecule degraders called PROTACs<sup>43</sup>. Our work established that RING domains constitute ligandable E3 ligases and therefore could be exploited for the development of PROTACs.

PRC1 complexes are essential chromatin regulators that are assembled in a combinatorial manner from various paralogs<sup>2,3,5,44</sup>. RING1B and RING1A are core subunits shared among highly diverse PRC1 complexes and are responsible for H2A ubiquitination activity as well as structural organization of PRC1 complexes. Our small molecule inhibitor RB-3 binds to the RING domains of RING1B and RING1A and inhibits E3 ligase activity of the canonical PRC1 complexes through disruption of the PRC1 interaction with chromatin. We expect that RB-3 will also bind to RING1A/B in non-canonical PRC1 complexes, which do not catalyze H2A ubiquitination<sup>5</sup>. Further studies are needed to assess how RB-3 impairs the activity of distinct polycomb complexes and availability of a direct PRC1 interaction inhibitor may serve as a valuable tool to study polycomb biology. Moreover, discovery of RB-3 might lead

to the development of therapeutically useful compounds targeting leukemic cells and possibly other cancers.

## Methods

### Expression and purification of recombinant proteins

RING1B-BMI1 and RING1A-BMI1 complexes were expressed either as fusion proteins (RING1B-BMI1f and RING1A-BMI1f) or heterodimer (RING1B-BMI1). Synthetic constructs encoding the fusion proteins encompassing RING1B (residues 10–116) and BMI1 (residues 1–104) or RING1A (residues 7–113) and BMI1 (residues 1–104) were ordered from Genscript and subcloned into the pET32a vector (Novagen). His<sub>6</sub>-thioredoxin RING1B-BMI1f and RING1A-BMI1f proteins were expressed in BL21 (DE3) *E. coli* cells grown in Luria broth (Sigma) or labelled M9 minimal media selected with ampicillin, and both proteins were purified in the same way. After 16 h induction with 0.5 mM isopropyl-β-D-thiogalactoside (IPTG) at 25°C cells were resuspended in lysis buffer containing 50 mM Tris, pH 7.5 at 25°C, 150 mM NaCl, 2 mM dithiothreitol (DTT), 100 μM ZnCl<sub>2</sub>, 0.5 mM phenylmethylsulfonyl fluoride (PMSF) and lysed using a cell disrupter. RING1B-BMI1f protein was solubilized from inclusion bodies and refolded through serial dialysis into refolding buffer (50 mM Tris, pH 7.5 at 25°C, 150 mM NaCl, 2 mM DTT, 100 μM ZnCl<sub>2</sub>). The His-thioredoxin tag was cleaved with TEV protease and separated from RING1B-BMI1f using cation exchange chromatography. The purified RING1B-BMI1f was exchanged into storage buffer (50 mM HEPES, pH 7.2, 100 mM NaCl, 10 mM MgCl<sub>2</sub>, 10 μM ZnCl<sub>2</sub>, 1 mM DTT) through dialysis. Labelled protein was dialyzed into NMR buffer containing 50 mM sodium phosphate, pH 6.8, 150 mM NaCl, 1 mM Tris(2-carboxyethyl)phosphine hydrochloride (TCEP), 10 μM ZnCl<sub>2</sub>. RING1B-BMI1f L94A and K85E mutants were generated using QuikChange site-directed mutagenesis protocol (Agilent) and purified as the RING1B-BMI1f.

To express non-covalent RING1B-BMI1 heterodimer, we cloned RING1B (residues 10–116) into pGST-parallel vector<sup>47</sup> and BMI1 (residues 1–104) was cloned into pHis-parallel vector<sup>47</sup>. Subsequently, DNA encoding pHis-BMI1 (1–104), containing RBS, His<sub>6</sub> tag, TEV recognition site, and BMI1 (1–104) sequence was amplified and inserted into pGST-RING1B (10–116) plasmid, to produce the bicistronic vectors. RING1B-BMI1 protein was expressed in BL21 (DE3) *E. coli* cells selected with ampicillin. After 18 h induction with 0.2 mM IPTG at 18°C cells were harvested by centrifugation and resuspended in lysis buffer containing 50 mM Tris, pH 7.5, 150 mM NaCl, 1 mM DTT, 100 μM ZnCl<sub>2</sub>, 0.5 mM PMSF and lysed using a cell disrupter. Clarified lysate was applied to Ni-NTA (Qiagen) affinity column. The column was extensively washed with lysis buffer containing 35 mM imidazole and eluted with lysis buffer containing 200 mM imidazole, and subsequently digested with TEV. The His<sub>6</sub> tag was removed using Ni-NTA column. Cleaved GST tag was removed by Superdex-75 size exclusion chromatography in buffer containing 50 mM tris pH 7.5, 100 mM NaCl, 1 mM TCEP.

## Expression and purification of RING ligases and UbcH5A

Plasmid for BRCA1 and BARD1 genes were kind gifts from Rachel Klevit (University of Washington, Department of Biochemistry) and proteins were expressed and purified as previously reported<sup>48</sup>. A synthetic gene encoding TRIM37 residues 1–90 was purchased from Genscript and subcloned into the pQE80L vector. His<sub>6</sub>-TRIM37 was expressed in BL21 (DE3) *E. coli* cells selected with ampicillin. After 16 hour induction with 0.2 mM IPTG at 18 °C cells were lysed by cell disruption and protein was purified using nickel affinity chromatography followed by Superdex-75 size exclusion chromatography in buffer containing 50 mM Tris pH 7.5, 100 mM NaCl, 1mM TCEP. Plasmids encoding RNF4 (residues 122–183), TRAF6 (residues 67–124), and TRIM31 (residues 1–66) with NcoI and EcoRI restriction sites were ordered from Genscript and subcloned into the modified pET32a bacterial expression vector (Novagene) containing thioredoxin tag and PreScission Protease cleavage site. Proteins were expressed and purified using nickel affinity chromatography followed by PreScission protease cleavage and removing the tag using nickel beads. RNF168 was a gift from Dr. Cheryl Arrowsmith (Addgene plasmid # 25298) and purified in a similar protocol as other E3 ligases. Plasmid encoding human UbcH5A was acquired from AddGene (#61081). Expression of and purification was performed using previously described protocol<sup>49</sup>.

## NMR-based fragment screen

We screened a library of 1000 commercially available fragment-like compounds by performing <sup>1</sup>H-<sup>15</sup>N HSQC experiments with 60 μM <sup>15</sup>N-labeled RING1B-BMI1f in a buffer containing 50 mM sodium phosphate, pH 6.8, 150 mM NaCl, 1 mM TCEP, 10 μM ZnCl<sub>2</sub>. Compounds were screened in mixtures of 20 compounds per sample at 250 μM final compound concentration, in 5% dimethyl sulfoxide (DMSO). <sup>1</sup>H-<sup>15</sup>N HSQC spectra were acquired at 30 °C on a 600MHz Bruker Avance III spectrometer equipped with cryoprobe, running Topspin version 2.1. Processing and spectral visualization was performed using NMRPipe v 3.0<sup>50</sup> and Sparky 3 v 3.113 (T. D. Goddard and D. G. Kneller, SPARKY 3, University of California, San Francisco).

## Assignment of RING1B-BMI1f backbone chemical shifts

Samples for backbone assignment were made with 400 μM <sup>13</sup>C<sup>15</sup>N-labeled RING1B-BMI1f and 430 μM <sup>2</sup>H,<sup>13</sup>C<sup>15</sup>N-labeled RING1B-BMI1f prepared in buffers containing either 50mM phosphate, 150mM NaCl, pH 6.5, 1mM TCEP, 5% D<sub>2</sub>O or 50 mM Tris, pH 7.5, 150 mM NaCl, 1mM TCEP and 5% D<sub>2</sub>O. Spectra were acquired at 30°C on a 600 MHz Bruker Avance III spectrometer equipped with cryoprobe, running Topspin version 2.1. Backbone assignment was done using a series of triple-resonance experiments including HNCACB, CBCA(CO)NH, HNCA, HN(CO)CA, HNCO, HN(CA)CO, and <sup>15</sup>N-separated NOESY-HSQC. Processing and spectral visualization was performed using NMRPipe v 3.0<sup>50</sup> and Sparky 3 v 3.113 (T. D. Goddard and D. G. Kneller, SPARKY 3, University of California, San Francisco).

## NMR binding studies

Samples for NMR binding studies were prepared with 60  $\mu\text{M}$   $^{15}\text{N}$  RING1B-BMI1f in buffer (50 mM sodium phosphate, pH 6.8, 150 mM NaCl, 1 mM TCEP, 10  $\mu\text{M}$   $\text{ZnCl}_2$ ) with compounds at various concentrations in 5% final DMSO and 7%  $\text{D}_2\text{O}$ . Compound binding was assessed by calculating the magnitude of chemical shift perturbations,

$\Delta_{\text{HN}} = \sqrt{(\delta_{\text{HN}}^2 + 0.1 * \delta_{\text{N}}^2)}$  (ppm) from  $^1\text{H}$ - $^{15}\text{N}$  HSQC spectra. Determination of  $K_{\text{D}}$  was based on the analysis of titration experiments using a binding isotherm adapted from<sup>51</sup>.

## Crystal structure determination

Crystals of RING1B-BMI1f were obtained using 8 mg/ml protein in 50 mM TRIS, pH 7.5, 300 mM NaCl, 1 mM TCEP and 100  $\mu\text{M}$   $\text{ZnCl}_2$  buffer and the precipitant solution (100 mM HEPES, pH 7.5 and 20% PEG 8000). X-ray diffraction data were collected from RING1B-BMI1f crystals on beamline 21-ID-G at LS-CAT (Advanced Photon Source, Argonne National Laboratory, USA). The collected data were processed, integrated, and scaled using the HKL2000 v 720 software package<sup>52</sup>. The structure was determined by molecular replacement method with the CCP4 version of MOLREP<sup>53</sup> using the BMI1/RING1B-UBCH5C complex structure (PDB ID: 3RPG) as a search model. Model building was performed with WinCoot<sup>54</sup> and refinement was carried out using PHENIX Refine<sup>55</sup>.

Co-crystallization of RING1B-BMI1f with RB-2 was performed with purified protein incubated with 6-fold molar excess compound at 4°C in 20 mM Tris pH7.5, 150 mM NaCl, 1 mM TCEP and concentrated to 9.8 mg/ml. Crystals were grown using the sitting drop vapor diffusion method at 4°C by mixing in a 1:1 ratio with a reservoir solution of 100 mM acetate pH 4.5, 200 mM  $\text{Li}_2\text{SO}_4$  and 2.5 M NaCl. Crystals obtained after 2 weeks were cryo-protected with additional 20% glycerol and then frozen in liquid nitrogen. X-ray diffraction data were collected on beamline 21-ID-F at LS-CAT (Advanced Photon Source, Argonne National Laboratory, USA). The data were processed as for RING1B-BMI1f using the HKL2000 software package<sup>52</sup> and structure was determined using molecular replacement with PHASER<sup>56</sup> followed by refinement using PHENIX Refine<sup>55</sup>.

Crystallographic data collection and refinement statistics are summarized in Supplementary Table 1. The final structures have been deposited in the Protein Data Bank (PDB) with the accession codes 6NBZ and 6NC0 for the RING1B-BMI1f and RING1B-BMI1f crystallized with RB-2, respectively.

## Characterization of the RING1B-BMI1f complex with RB-2 using NMR

For structural studies of RING1B-BMI1f and RB-2 we expressed  $^2\text{H}$ ,  $^{13}\text{C}$ ,  $^{15}\text{N}$  labeled RING1B-BMI1f with  $^1\text{H}$  methyl labeled Ile, Val and Leu (DCN ILV RING1B-BMI1f) using a previously described protocol<sup>57</sup>. For NMR experiments, we prepared samples consisting of 120  $\mu\text{M}$  DCN ILV RING1B-BMI1f with 500  $\mu\text{M}$  RB-2 in 50 mM sodium phosphate, pH 6.8, 150 mM NaCl, 1 mM TCEP, 10  $\mu\text{M}$   $\text{ZnCl}_2$  buffer with 5% DMSO. Protein assignment was based on backbone assignment for RING1B-BMI1f and side chains were assigned using 3D HCCH-TOCSY and 3D  $^{13}\text{C}$ -separated HSQC-NOESY with 350 ms mixing time. RB-2 assignment was obtained from 2D NOESY and 2D TOCSY spectra.

Modeling of the RING1B-BMI1f complex with RB-2 was performed using the HADDOCK2.4 docking routines<sup>24</sup>. We employed the crystal structure of RING1B-BMI1f obtained in the presence of RB-2 as the protein receptor. Coordinate and parameter files for RB-2 were generated with PRODRG server. Intermolecular NOEs were determined from 3D <sup>13</sup>C separated NOESY with 350ms mixing time and the following list of NOE-based distance restraints were employed in the calculations: I77 δ1CH<sub>3</sub> – H1; I77 δ1CH<sub>3</sub> – H3; I77 δ1CH<sub>3</sub> – H13; I77 δ1CH<sub>3</sub> – H14; L94 δ1/δ2CH<sub>3</sub> – H10, L94 δ1/δ2CH<sub>3</sub> – H11, L94 δ1/δ2CH<sub>3</sub> – H12, L94 δ1/δ2CH<sub>3</sub> – H13, L94 δ1/δ2CH<sub>3</sub> – H14; L100 δ1/δ2CH<sub>3</sub> – H7, L100 δ1/δ2CH<sub>3</sub> – H10, L100 δ1/δ2CH<sub>3</sub> – H11, L100 δ1/δ2CH<sub>3</sub> – H12, L100 δ1/δ2CH<sub>3</sub> – H13, L100 δ1/δ2CH<sub>3</sub> – H14.

The ambiguous interaction restraints (AIRs) were obtained from the joint analysis of ligand induced chemical shift changes on the protein structure and the RING1B-BMI1f crystal structures obtained in the presence and the absence of RB-2 ligand. Labeling of RB-2 protons is shown in Supplementary Fig. 2f. All NMR-derived distance restraints were defined as unambiguous restraints using a bounded constraint function between 2.2 and 5.25 Å distance. 200 models of RING1B-BMI1f with docked RB-2 were generated using CNS1.3 utilizing the HADDOCK2.4 mediated docking algorithms against combined experimental crystal structure and solution NMR data sets. The 200 structure models were generated from independent simulations and the top twenty models with the lowest overall HADDOCK energy term were selected for further analysis. Structural statistics are reported in Supplementary Table 2 and the final set of the structure has been deposited in the Protein Data Bank (PDB) with the accession code 7ND1.

### ITC experiments

RING1B-BMI1f was exchanged into ITC buffer (50 mM phosphate, pH 6.8, 100 mM NaCl, 1 μM ZnCl<sub>2</sub>, 1 mM TCEP) by gel filtration and degassed prior to measurement. The titrations were performed using a VP-ITC titration calorimetric system (MicroCal) at 25°C. The calorimetric cell, containing RING1B-BMI1f (26.6 μM) with 5% DMSO, was titrated with RB-3 (270 μM in 5% DMSO) injected in 10 μL aliquots. Reference cell contained buffer with 5% DMSO. Data were analyzed using Origin 7.0 (OriginLab) to obtain K<sub>D</sub> and stoichiometry.

### AlphaScreen competition assay

For AlphaScreen competition assay experiments, 50 nM His<sub>6</sub>-RING1B-BMI1f and 10 nM biotinylated recombinant human mononucleosomes (EpiCypher) were incubated in assay buffer containing 50 mM Tris pH 7.5, 150 mM NaCl, 1 mM TCEP, 0.025% Tween-20, 0.01% bovine serum albumin (BSA) for 1 hour at room temperature in 384-well Alpha Plates (PerkinElmer). Compounds were added to a final concentration of 5% DMSO and incubated for 1 hour at room temperature. Nickel Chelate Acceptor beads (PerkinElmer) were added to a final concentration of 20 μg/mL and incubated for 1 hour at room temperature. Streptavidin Donor beads (PerkinElmer) were added to a final concentration of 20 μg/mL and incubated for 2 hours at room temperature. Luminescence was measured as AlphaSignal on a Pherastar FS microplate reader (BMG Labtech) and data was fit in Prism 8.0 (GraphPadSoftware Inc., v 821 (441)).

## Nucleosome preparation

Plasmids for *Xenopus* histones and the 147 bp Widom 601 sequence were kind gifts from Dr. Yali Dou (University of Michigan Department of Pathology). Histones H2A, H2B, H3 and H4 were expressed in CodonPLUS BL21 (DE3) *E. coli* cells (Sigma) and with ampicillin selection. After 4 hour with 0.4 mM IPTG at 37°C cells were resuspended in lysis buffer A containing 50 mM Tris, pH 7.5 at 25°C, 100 mM NaCl, 1 mM disodium ethylenediaminetetraacetate dihydrate (Na-EDTA), 1 mM PMSF, 1 mM  $\beta$ -mercaptoethanol ( $\beta$ -ME) and lysed using a cell disrupter. Histone proteins were isolated from inclusion bodies and solubilized proteins were further purified using anion and cation exchange before dialysis into excess MilliQ water with 2 mM  $\beta$ -ME at 4°C. Samples were clarified and lyophilized. Histone octamer was prepared from lyophilized histone proteins resuspended in histone unfolding buffer (8 M guanidine hydrochloride, 20 mM Tris pH, 7.5, 5 mM DTT) before mixing in a 1:1:1:1 molar ratio to a final protein concentration of 2 mg/mL. Histone mixture was dialyzed overnight into 2,000-fold excess octamer reconstitution buffer (2 M NaCl, 10 mM Tris, pH 7.5, 1 mM EDTA, 5 mM  $\beta$ -ME). Homogeneous octamer was purified via size exclusion chromatography using a Sephacryl S200 column (GE Healthcare) with octamer reconstitution buffer. The 147 base pair 601 DNA was prepared from EcoRV digestion of plasmid containing 23 tandem repeats of 601 DNA. Purified 601 DNA and histone octamer were mixed in varying molar ratios at 0.7 mg/mL final DNA concentration in high salt nucleosome reconstitution buffer (2 M NaCl, 20 mM Tris, pH 7.5, 1 mM EDTA, 1 mM DTT) and nucleosomes were reconstituted by serial dilution from 2M NaCl to final concentration of 200 mM. Reconstituted nucleosomes were dialyzed into the EMSA assay buffer (50 mM HEPES, pH 7.2, 100 mM NaCl, 10 mM MgCl<sub>2</sub>, 1  $\mu$ M ZnCl<sub>2</sub>, 1 mM DTT). Nucleosome quality was assessed by pre-electrophoresed 7.5% tris-glycine native-PAGE. H2B<sub>OG488</sub> nucleosomes were prepared as above with the exception that H2B S112C was labeled with OregonGreen 488 maleimide (Invitrogen) prior to octamer assembly.

## EMSA assay

RING1B-BMI1f was diluted to 1  $\mu$ M final concentration in EMSA buffer (50 mM HEPES, pH 7.2, 100 mM NaCl, 10 mM MgCl<sub>2</sub>, 1  $\mu$ M ZnCl<sub>2</sub>, 1 mM DTT, 5% glycerol, 0.01% BSA) and incubated with varying concentrations of compound at room temperature for 90 minutes. H2B<sub>OG488</sub> nucleosomes were added to a 10 ng/ $\mu$ L final concentration in 10  $\mu$ L reaction and reactions were incubated at room temperature for 30 minutes. 1  $\mu$ L DNA loading dye was added to each reaction (Life Technologies). Reaction species were separated by electrophoresis at 4° C under native conditions using 7.5% Tris-glycine acrylamide gel (BioRad). Gels were imaged with Typhoon Trio+ 9410 Variable Mode Imager (GE Healthcare) and analyzed with ImageQuant TL 7.0 (GE Healthcare).

## In Vitro Ubiquitination Assay

The *in vitro* ubiquitination reaction was carried out in a 25- $\mu$ L reaction volume containing E3 ligase reaction buffer, 50 mM HEPES pH 7.2, 100mM NaCl, 10 mM MgCl<sub>2</sub>, 1 mM DTT, and 1  $\mu$ M ZnCl<sub>2</sub> with 10  $\mu$ M of Flag-tagged ubiquitin (Cat. No. U-115), 10 nM of UBE1 (Cat. No. E305), and 1.5  $\mu$ M of UbcH5A (Cat. No. E2-616; all from Boston Biochemicals), 3mM adenosine 5'-triphosphate, 250 ng of purified HeLa nucleosomes (HMT-35-123,

Lot#1809, Reaction Biology) and between 20 and 100 nM of purified heterodimeric RING1B-BMI1, RING1B-BMI1f or RING1A-BMI1f as an E3 ligase. In first step of reaction, E3 ligase reaction mix without Nucleosomes or Flag-ubiquitin was incubated with different concentrations of compounds for 30 minutes at room temperature. Subsequently, HeLa nucleosomes and Flag-ubiquitin were added to individual reactions and the whole reaction was incubated at 37°C for 60 minutes. The in-vitro ubiquitination reactions using TRIM37 [buffer: 50 mM Tris-Cl, pH 7.9, 5 mM MgCl<sub>2</sub>, 2 mM NaF, 1 mM DTT and 2 mM ATP] and BRCA1-BARD1 [buffer: 50 mM Tris-HCl pH 7.5, 2.5 mM MgCl<sub>2</sub>, 15 mM KCl, 0.7 mM DTT, 0.01% Triton, 1% glycerol and 2 mM ATP] were performed as described above for RING1B-BMI1. The reactions were terminated by addition 4x SDS gel loading dye and analyzed by running the proteins in 12% SDS-PAGE and subjected to immunoblotting with H2Aub(K119) (Cell Signaling Technology #8240S, clone D27C4, dilution 1:3000), H3 (Cell Signaling Technology #9715, dilution 1:20000) and FLAG (F1804, Sigma, dilution 1:2000). The *in vitro* ubiquitination with RNF168 was performed using the following conditions: E1 (200 nM); E2-UbcH5c (1 μM), E3 (10 μM), ATP (3 mM), Flag-ubiquitin (20 μM), recombinant H2A (1 μM); incubated for 16 hours at 32 °C in 50 mM HEPES pH 7.2, 100 mM NaCl, 10 mM MgCl<sub>2</sub>, 1 uM ZnCl<sub>2</sub>, 1 mM DTT buffer<sup>27</sup>. Immunoblotting was performed with anti-H2A antibody (Millipore Sigma #07-146, dilution 1:1000).

### Profiling RB-3 selectivity

Kinase profiling was performed by Nanosyn and the activity of RB-3 was tested at 25 μM using selected protein kinases. Profiling of the RB-3 activity against a panel of epigenetic proteins including HDACs, sirtuins, bromodomains and chromodomains was performed by Reaction Biology using 25 μM BT5 and 1 h incubation time. Activity of RB-3 against histone methyltransferases was tested by radiometric assays for a panel of recombinant SET domains as reported in<sup>58</sup> using 25 μM BT5 and 1 h incubation time.

To test binding of RB-3 to DNA we employed NMR spectroscopy. 16 bp oligonucleotides AGGACCGGAAGTAACT and the complementary AGTTACTTCCGGTCCT were ordered from IDT, dissolved in water, annealed and prepared in 50 mM Tris pH 7.5, 50 mM NaCl buffer. NMR experiments were performed using 50 μM oligo titrated with 50 μM RB-3 or Doxorubicin.

### Cell lines, Cell culture and Primary AML patient samples

The MV4;11, MOLM13, K562, HEK293T and HeLa cell lines were obtained from ATCC while TEX and MLL-ENL were kind gift from Dr. John Dick, University of Toronto. MV4;11, MOLM13 and K562 cells were maintained in RPMI-1640 media with 10% fetal bovine serum (FBS) and 1% penicillin/streptomycin (Gibco). TEX and M9-ENL1 were cultured in Iscove's Modified Dulbecco's Medium (IMDM) media containing human SCF, IL-3 and IL-7 as described previously<sup>37</sup>. HEK293T and HeLa cells were cultured in Dulbecco's Modified Eagle Medium (DMEM) media with 10% FBS and 1% penicillin/streptomycin (Gibco). All cell lines were used in the described experiments before reaching the 10<sup>th</sup> passage after thawing the cells out. Patient-derived AML samples were collected in accordance with the guidelines and approval of institutional review boards at Weill Cornell

Medical College, New York and the University of Pennsylvania, and informed consent from each patient. Peripheral blood samples were collected and processed to isolate mononuclear cells using density gradient centrifugation and red blood cell lysis. Cells were frozen in 10% DMSO until used in experiments. CD34 positive bone marrow blood cells were obtained from Allcells (ABM021F) and stored in liquid nitrogen until use. For > 4 days treatment experiments, media were changed at day 3–4 interval, with the viable cell numbers restored to the original concentration in the DMSO treated samples and using the same dilution factor for cells treated with compounds, unless otherwise indicated; compounds were re-supplied each time during media change.

### Live cells NanoBiT assay

NanoLuc® Binary Technology (NanoBiT) assays were performed with  $2 \times 10^5$  cells/ml HEK293T cells transiently transfected with 1  $\mu$ g/ml of the N-LgBiT-RING1B plasmid (full length RING1B or RING1B R98A cloned into pBiT1.1-N[TK LgBiT vector, Promega) and 0.25  $\mu$ g/ml of the SmBiT-H3.3 plasmid (CMV/H3.3-SmBiT vector, Promega), and 7:1 FuGENE® HD Transfection Reagent-to-DNA ratio (Promega) in Opti-MEM™ (Gibco). After 24 h, cells were trypsinized and transferred to white 96-well tissue culture plates (30,000 cells in 100  $\mu$ l per well) and incubated with compounds or 0.25% DMSO. After another 24 h, 25  $\mu$ l of Nano-Glo® Live Cell Assay System (Promega) were added to each well and NanoLuc® Luminescence was detected in a PHERAstar BMG microplate reader.

### Pull-down experiments with biotinylated compounds

HEK293T cells were lysed using 500  $\mu$ L lysis buffer (Phosphate buffered saline (PBS) adjusted to 500 mM NaCl, 1% Triton X-100, 1X protease inhibitor cocktail) and flash frozen with liquid nitrogen. Lysate was thawed, diluted to 1 mg/mL and pre-cleared with streptavidin magnetic beads (New England BioLabs Inc.) for 1 hour at 4°C on a rotating rack. Biotinylated compounds RB-3-biot and RB-nc-biot were incubated with beads for three hours following with incubation with cell lysate overnight at 4°C. The following day the beads were washed 10 times with wash buffer (PBS adjusted to 500 mM and 0.1% Triton X-100) with vortexing at each washing step. Washed beads were resuspended in 1X SDS dye and boiled for 15 minutes. The samples were separated by SDS-PAGE and transferred to a nitrocellulose membrane. Detection by immunoblotting used 1:1,000 monoclonal RING1B (Cell Signaling Technology #5694S) and 1:20,000 HRP-linked anti-rabbit IgG (Cell Signaling Technology #7074S); and 1:1,000 monoclonal BMI1 (Cell Signaling Technology #6964S) and 1:10,000 HRP-linked anti-mouse IgG (Cell Signaling Technology #7076S).

### Cell viability assay

$1 \times 10^5$  cells/ml TEX cells were plated in 24-well plates and treated with the compounds or 0.25% DMSO followed by incubation at 37°C for 4 or 8 days. For experiments with PTC209,  $1 \times 10^5$  cells/ml TEX cells were plated in the 12-well plate in duplicates and treated with different doses of PTC209 or 0.25% DMSO followed by incubation at 37°C for 4 days. Before read-out, 100  $\mu$ l of cell suspensions were transferred to 96-well plates for each sample in quadruplicates, and the MTT cell proliferation assay kit (Roche) was applied. Absorbance was detected at 570 nm using a PHERAstar BMG microplate reader. The

experiments were performed two to three times in quadruplicate with calculation of mean and standard deviation for each condition.

### Immunoblotting

Whole cell lysates were prepared using RIPA lysis buffer (Thermo Scientific) containing 1X protease inhibitor cocktail (Sigma) according to standard protocol and quantitated using BCA protein assay kit (Thermo Scientific). A total of 10 to 20ug of whole cell lysates were separated on either 10%, or 12% SDS-PAGE precast gels (Invitrogen) and was transferred onto nitrocellulose membrane (Millipore). All blots were probed with primary antibodies specific overnight at 4 °C, and with the appropriate HRP-conjugated secondary antibody for 1 h at room temperature. Membranes were visualized on autoradiography film after incubating with ECL reagent (ECL Prime, GE Healthcare). Antibodies used in this study include histone H2Aub (K119), (Cell Signaling Technology #8240S, clone D27C4, dilution 1:25000), histone H2A (Cell Signaling Technology #12349S, dilution 1:5000), RING1B (Santacruz, N-32, SC101109, dilution 1:1000), RING1A (Cell Signaling Technology #13069S, dilution 1:1000), BMI1 (05-637, cloneF6, EMD Millipore, dilution 1:1000), histone H3(ab1791, abcam, dilution 1:25000), histone H2Bub (Cell Signaling Technology #5546S, dilution 1:10000),  $\beta$ -Actin (A00702, GenScript, dilution 1:50000), CEBP $\alpha$  (Cell Signaling Technology #2295S, dilution 1:1000) and secondary antibodies goat anti-mouse IgG-HRP (Cell Signaling Technology #7076S, dilution 1:10000) and goat anti-rabbit IgG-HRP (Cell Signaling Technology #7074S, dilution 1:20000).

### RNA interference

100,000 HeLa or K562 cells were reverse transfected with 25 nM of Control and RING1B/BMI1 siRNA (Dharmacon) for 96 hours using lipofectamine RNAiMax (Invitrogen) as per manufacturer instructions in 6 well plates. Cells were incubated for 96 hours before washing, trypsinization and lysis. Equal amounts of whole cell lysate were separated on 10% or 12% SDS-PAGE gels and analyzed by immunoblotting as described.

### RNAseq studies

$0.2 \times 10^6$  cells/ml TEX cells were plated in 12-well plates and treated with 25 $\mu$ M RB-3 or 0.25% DMSO in triplicates. Cells were harvested after 6 and 10 days of treatment. Total RNA was isolated with RNeasy Mini kit (Qiagen), and the quality of RNA was assessed by the TapeStation (Agilent). Next Generation Sequencing was performed at the University of Michigan Advance Genomics Core. Samples with RNA Integrity Numbers (RINs)  $\geq 8$  were selected to make RNA-seq library. The Illumina TruSeq mRNA kit (Illumina) was used to construct the library. mRNA was isolated with polyA beads. RNA-seq libraries was sequenced with Hiseq2000 platform. Sequencing Reads were aligned to hg19 with Bowtie2.0 and Tophat (version 2.0.3). Cuffdiff was used to determine differential gene expression analysis. Genes with  $p < 0.05$  and a 2-fold change was considered significant. Gene Set Enrichment Analysis (<http://www.broadinstitute.org/gsea/index.jsp>) was performed on gene expression of RB-3 treated versus DMSO treated cells.

### Real-time qPCR

$0.2 \times 10^6$  cells/ml TEX cells were plated in 12-well plate in duplicates and treated with RB-3 and/or RB-nc for 6 and/or 10 days followed by RNA isolation according to the manufacturer's protocol (RNeasy kit Qiagen). For PTC-209,  $0.2 \times 10^6$  cells/ml TEX cells were plated in 12-well plate in duplicates and treated with different doses of PTC-209 for 4 days followed by RNA isolation according to the manufacturer's protocol (RNeasy kit Qiagen). 250ng to 1 $\mu$ g of total RNA was then reverse transcribed to cDNA using HICAP RT kit (Applied Biosystems). Following cDNA synthesis, quantitative PCR was performed using SYBR Green Supermix with ROX (BioRad) using the primers for *CEBPA*, *CD34*, *CD86*, *ITGAM*, *CD48*, *MS4A3*, *TIMP3*, *GAPDH*, *RNASE2* and *CCNA1* (see Supplementary Info for primer sequences). Gene expression analysis was carried out using the  $2^{-CT}$  relative quantification method. Duplicate reactions were performed for each tested sample, and the average CT was calculated for the quantification analysis. GAPDH was used as an endogenous reference control. Primary AML samples treated with RB-3 and RB-nc for 12 days were processed in similar manner to isolate RNA, perform cDNA synthesis and quantitative analysis of *CEBPA*, *CD34*, *ITGAM* and *CD86*.

### Chromatin Immunoprecipitation

$1.5 \times 10^6$  TEX cells plated in 10 cm dish were treated with 0.25% DMSO or RB-3 and RB-nc at 25  $\mu$ M concentrations. Following 8 days of incubation, cells were fixed with 1% paraformaldehyde for 10 min at room temperature. Cells were then quenched with glycine for 5 min at room temperature. ChIP was performed using SimpleChIP® Enzymatic Chromatin IP Kit (Cell Signaling Technology; #9003) according to the manufacturer's instructions. The DNA-protein complexes (from  $4 \times 10^6$  cells) treated with DMSO or RB-3 and RB-nc were immunoprecipitated using antibodies against H2Aub (K119) (Cell Signaling Technology #8240S, clone D27C4, 5  $\mu$ l per 40  $\mu$ l chromatin), RING1B (39663, Active Motif, 5  $\mu$ l per 40  $\mu$ l chromatin), H3 (Cell Signaling Technology #4620S, clone D2B12, 5  $\mu$ l per 40  $\mu$ l chromatin), H3K4me3 (Cell Signaling Technology #9751S, 5  $\mu$ l per 40  $\mu$ l chromatin) and normal IgG (Cell Signaling Technology #2729P, 5  $\mu$ l per 40  $\mu$ l chromatin) overnight at 4°C. The DNA was eluted using SimpleChIP® Enzymatic Chromatin IP Kit (Cell Signaling Technology; #9003) according to the manufacturer's instructions and subjected to qPCR using SYBR Green promoter region primers for *CEBPA*, *CD34* and *CD11b* (see Supplementary Information for primer sequences).

### ChIP-seq experiments

For ChIP experiments,  $3 \times 10^6$  TEX cells plated in 75mm culture flask were treated with 0.25% DMSO or 25  $\mu$ M RB-3 for 6 days. On day 6 cells were processed for ChIP sequencing following the standard protocol provided by Active Motif. Briefly,  $25-30 \times 10^6$  TEX cells were fixed with 1% formaldehyde for 15 min and quenched with 0.125 M glycine. Cells were centrifuged, washed and pellets were stored in  $-80^\circ\text{C}$  until their processing at Active Motif facility, CA. Chromatin was isolated, followed by disruption with a Dounce homogenizer. Lysates were sonicated with Bioruptor Plus. ChIPed DNA was isolated by treating aliquots of chromatin with RNase, proteinase K. Input was incubated at 55 degree for de-crosslinking. DNA was isolated by ethanol precipitation.

An aliquot of chromatin (30  $\mu\text{g}$ ) was precleared with protein A agarose beads (Invitrogen). Genomic DNA regions of interest were isolated using 5  $\mu\text{g}$  of antibody against H2AK119Ub (CST, cat 8240, Lot 6). *Drosophila melanogaster* chromatin was “spiked-in” to each reaction as a minor fraction of total chromatin to normalize ChIP-Seq data<sup>59</sup>. Spike-in created a normalization factor which was applied to the sample genome. Chromatin complexes were washed, then eluted from the beads with SDS buffer. Beads chromatin complexes were de-crosslinked overnight at 65 C. ChIPed DNA was purified by phenol-chloroform extraction and ethanol precipitation at  $-20$  C overnight. qPCR reactions targeting specific genomic regions with SYBR Green Supermix (Bio-Rad) were performed in triplicate.

Illumina sequencing libraries were prepared from the ChIP and Input DNAs by the standard consecutive enzymatic steps of end-polishing, dA-addition, and adaptor ligation. After a final PCR amplification step, the resulting DNA libraries were quantified and sequenced on Illumina’s NextSeq 500 (75 nt reads, single end). Reads were aligned to the human genome (hg19) using the BWA algorithm (default settings). Duplicate reads were removed and only uniquely mapped reads (mapping quality  $\geq 25$ ) were used for further analysis. Alignments were extended in silico at their 3’-ends to a length of 200 bp, and assigned to 32-nt bins along the genome. H2AK119Ub enriched regions were identified using the SICER algorithm at a cutoff of FDR  $1\text{E}-10$  and a max gap parameter of 600 bp. Peaks that were on the ENCODE blacklist of known false ChIP-Seq peaks were removed. Signal maps and peak locations were used as input data to Active Motifs proprietary analysis program, which creates Excel tables containing detailed information on sample comparison, peak metrics, peak locations and gene annotations.

### Flow cytometry experiments

Cells and primary AML samples treated with RB-3 and RB-nc were collected, washed once with 1 mL flow cytometry buffer (PBS with 1% FBS), and stained with antibodies to human CD34-APC/CY7 (1:100; 343514, BD BioLegend), CD38-PE (1:100; 12-0388-42, eBiosciences), CD11b-Pacific Blue (1:100; 301315, BioLegend) and CD86-Super Bight 436 (1:100; 62-0869-41, eBioscience). Cells were then analyzed using an LSR II flow cytometer (BD Bioscience) collecting at least  $2 \times 10^5$  events for each sample. Data analysis was performed using FlowJo 10.0.8 software for Windows 7 (TreeStar).

### Colony Formation assays

$0.5$  to  $1 \times 10^4$  cells/mL cells were plated in duplicate on methylcellulose medium supplemented with human cytokines (Methocult H4435; STEMCELL). RB-3 and RB-nc or DMSO were added to the methylcellulose and incubated at  $37^\circ\text{C}$ , 5%  $\text{CO}_2$ , for 7 days, at which time colonies were counted, harvested and replated with fresh methylcellulose and inhibitors and DMSO at initial density for another 7 days and counted. For colony formation assay in primary AML patient samples, samples were thawed and cultured for 6–24 hrs in IMDM with 20% BIT9500 (9500, STEMCELL), 50 ng/mL SCF, 20 ng/mL IL-3, 20 ng/mL IL6, 50 ng/mL FLT3L, 20 ng/mL GM-CSF and 20 ng/mL G-CSF (PeproTech), LDL 3.34  $\mu\text{L}/\text{mL}$  (STEMCELL). Cells were processed similarly as described for MLL-ENL1 cells, with cell density of 25,000–50,000 cells/mL in MethoCult Express (4437, STEMCELL) in 35 mm dishes (cat # 27100, STEMCELL).

Colony assays using normal CD34<sup>+</sup> cells were performed using a similar protocol. Briefly, frozen CD34<sup>+</sup> cells were thawed and cultured in IMDM medium with 20% BIT9500 (9500, STEMCELL), 100 ng/mL SCF, 20 ng/mL IL-3, 20 ng/mL IL6, 10 ng/mL FLT3L, 20 ng/mL GM-CSF and 20 ng/mL G-CSF (Peprotech). Then 750 cells/mL CD34<sup>+</sup> cells were plated in MethoCult Express (4437, STEMCELL) with RB-3 or DMSO and cultured in 35 mm dishes (27100, STEMCELL). The number of colonies was counted after 7–10 days and cells were re-plated for the second round.

Primary samples were thawed and cultured in IMDM with 20% BIT9500 (9500, STEMCELL), 50 ng/mL SCF, 20 ng/mL IL-3, 20 ng/mL IL6, 50 ng/mL FLT3L, 20 ng/mL GM-CSF and 20 ng/mL G-CSF (Peprotech), LDL 3.34  $\mu$ L/mL. Compounds dissolved in DMSO were added to cells at the density of 25,000–50,000 cells/mL in MethoCult Express (4437, STEMCELL) in 35 mm dishes (cat # 27100, STEMCELL). The number of colonies was counted after 7–10 days and two rounds of colony assays were performed.

### Cytospin/Wright-Giemsa staining

$1 \times 10^5$  cells/ml TEX cells were plated in 24-well plates and treated with the RB-3 and RB-nc or 0.25% DMSO followed by incubation at 37°C for 21 days. On day 21 cytopspins were prepared as described previously<sup>60</sup>. Analysis of the primary AML cells was performed following the treatment in colony assay. The cells were washed with PBS twice, and approximately  $1 \times 10^5$  cells were used for cytopspin and Wright-Giemsa staining.

**Statistical Analysis**—Student's t test (unpaired, two-tailed) was used to calculate significance level between treatment groups in all experiments. A p value < 0.05 was considered significant. Graph generation and statistical analysis were performed using GraphPad Prism version 8.2.1 (441) software (GraphPad Software).

### Chemistry

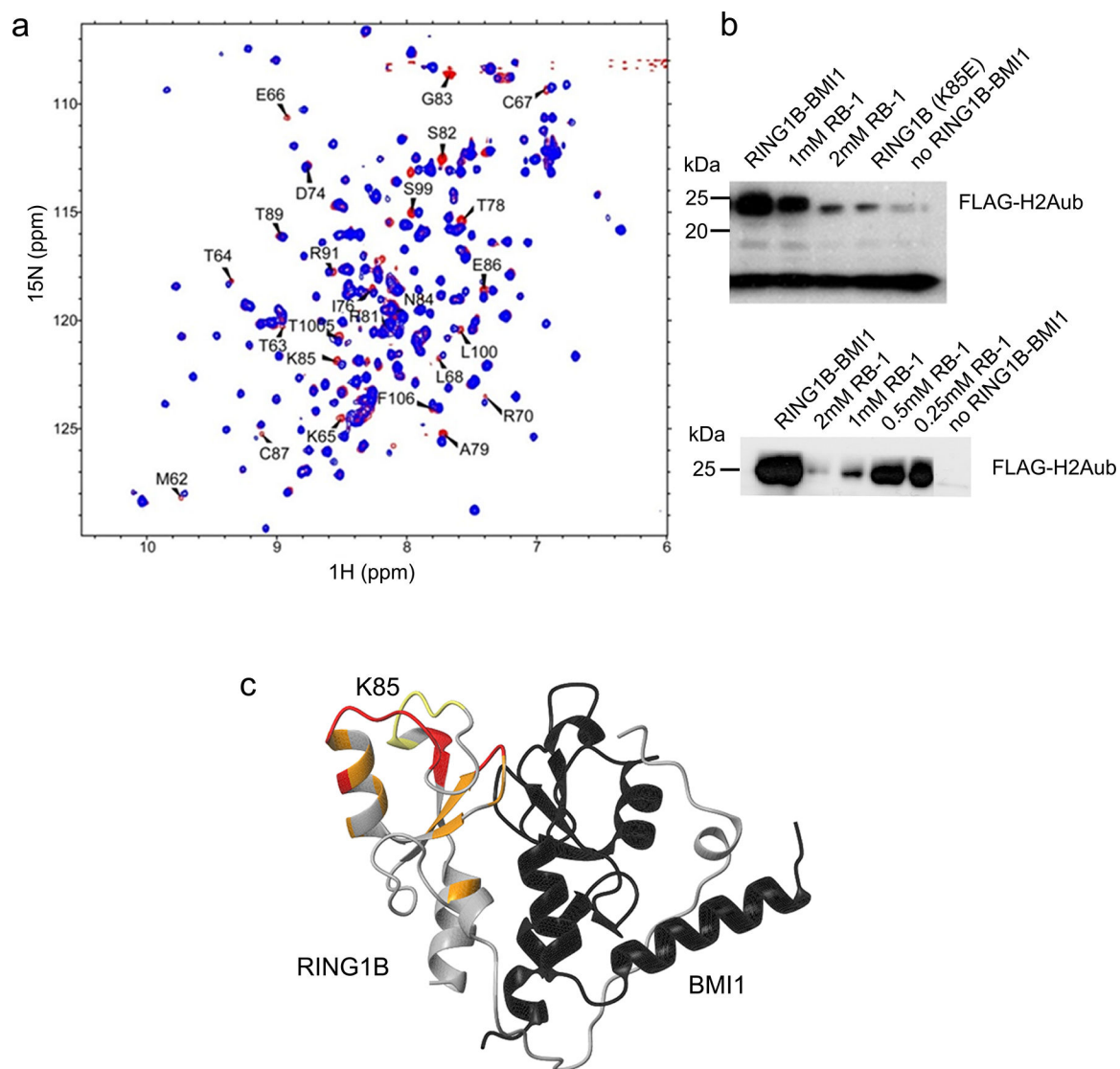
Detailed description of chemistry methods and characterization of compounds is included in Supplementary Data.

**Reporting summary.**—Further information on research design is available in the Nature Research Reporting Summary linked to this article.

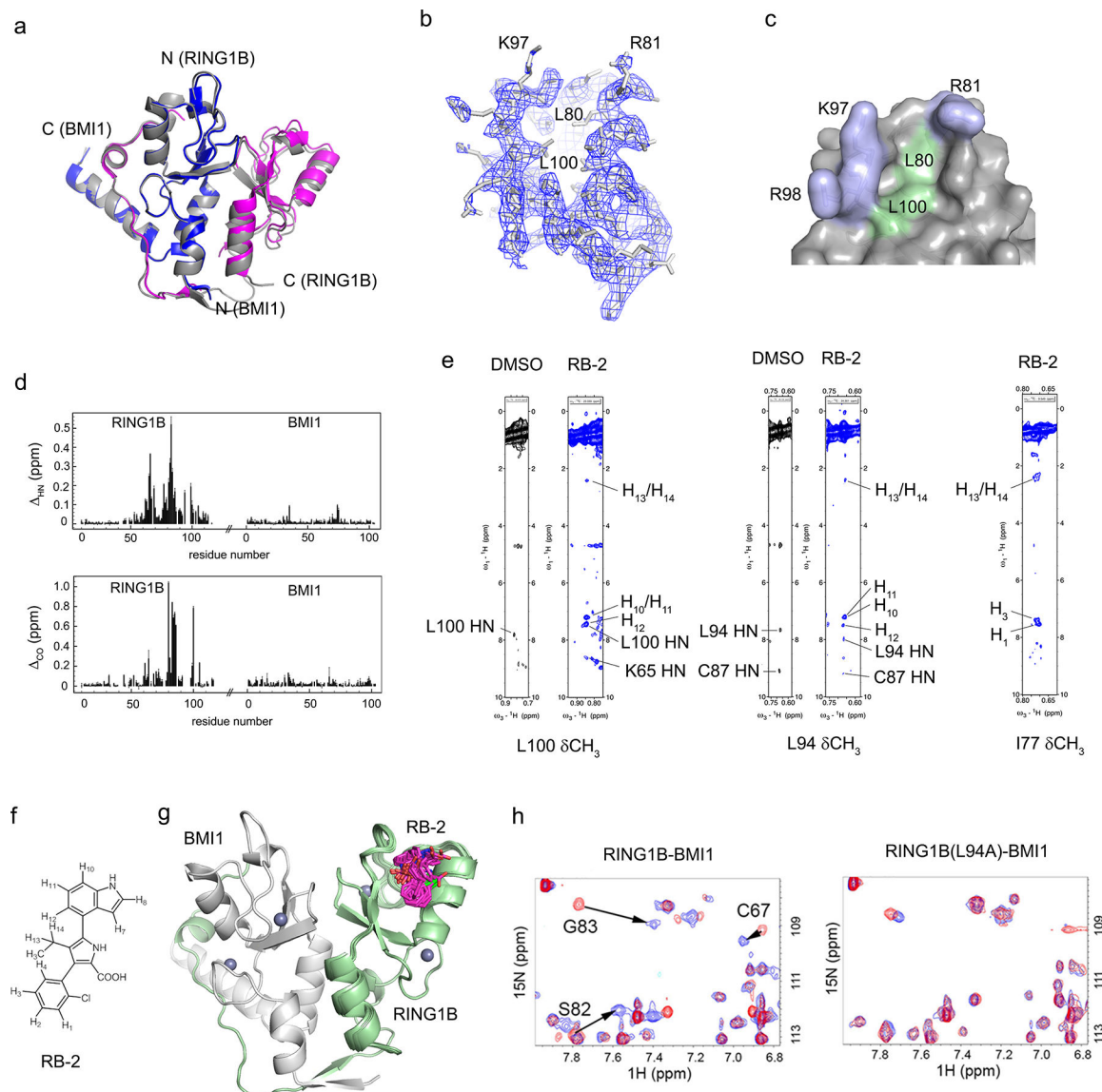
### Data availability

RNA-seq and ChIP-seq data for TEX cells treated with RB-3 have been submitted to GEO database under accession codes GSE123490 and GSE123930, respectively. Structure of RING1B-BMI1f and RING1B-BMI1f co-crystalized in the presence of RB-2 were deposited in PDB under the accession codes 6WI7 and 6WI8, respectively. Structure of RING1B-BMI1f-RB-2 complex determined using hybrid approach was deposited in PDB under the accession code 7ND1. PDB structures 3RPB and 4R8P were used for data analysis.

## Extended Data

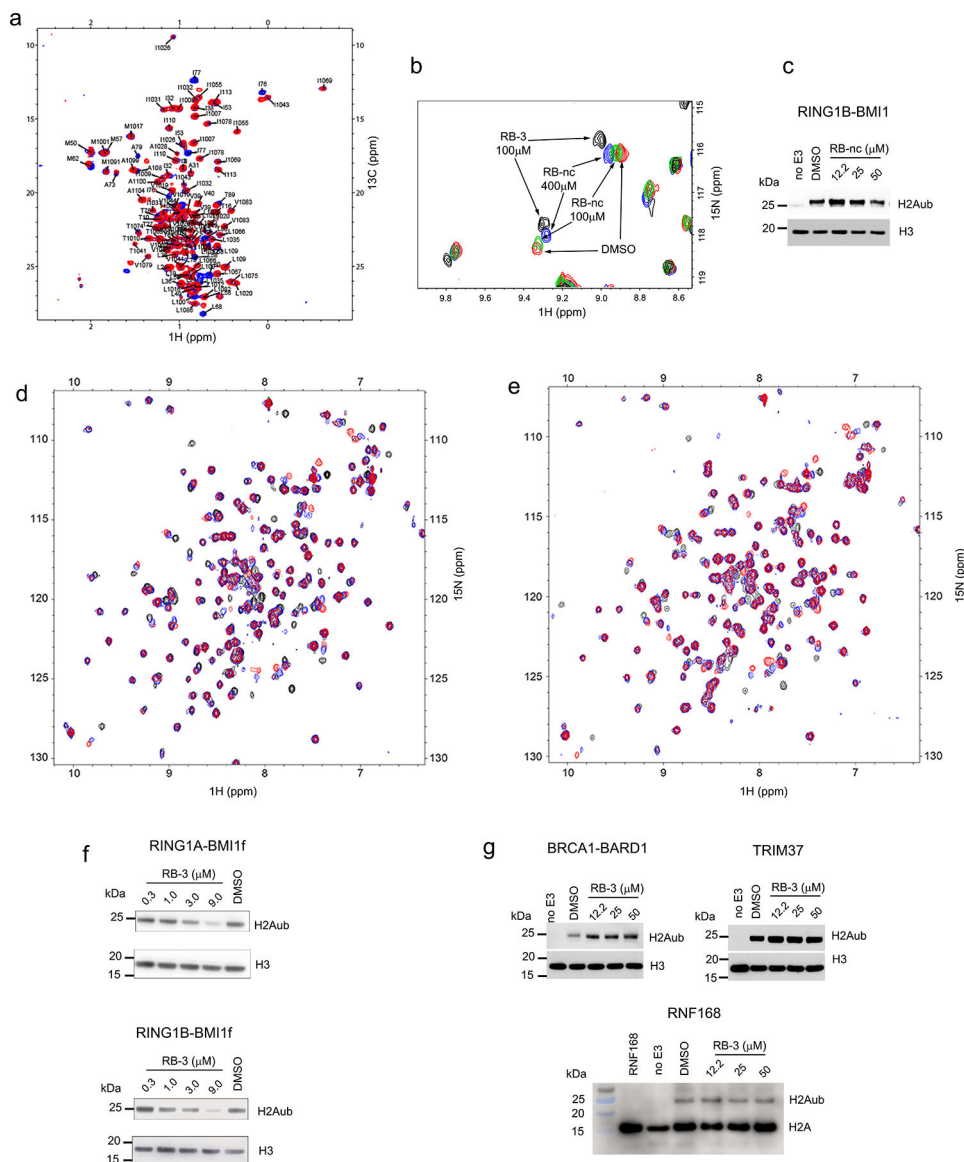
**Extended Data Fig. 1. Identification and characterization of fragment hit RB-1.**

**a)**  $^1\text{H}$ - $^{15}\text{N}$  HSQC spectrum of  $80\ \mu\text{M}$   $^{15}\text{N}$  RING1B-BMI1f (blue) superimposed onto  $80\ \mu\text{M}$   $^{15}\text{N}$  RING1B-BMI1f with  $2\ \text{mM}$  RB-1 (red). Several residues with the largest chemical shift perturbations are labeled. **b)** *In vitro* ubiquitination assay showing inhibition of RING1B-BMI1f E3 ligase activity with RB-1. Purified HeLa nucleosomes were incubated with E1 (UBE1), E2 (UBCH5C), E3 (RING1B-BMI1f), ATP and FLAG-tagged ubiquitin. Blots were probed with antibody against FLAG. RING1B (K85E) corresponds to the assay with RING1B(K85E)-BMI1 mutant. Assay was repeated 2 times (top and bottom immunoblots). **c)** Mapping of chemical shift perturbations  $\delta_{\text{HN}}$  (ppm) determined upon binding of  $2\ \text{mM}$  RB-1 to  $80\ \mu\text{M}$  RING1B-BMI1f. Residues are colored as follows:  $\delta_{\text{HN}} < 0.01$  (yellow);  $0.01 < \delta_{\text{HN}} < 0.04$  (orange);  $\delta_{\text{HN}} \geq 0.04$  (red). BMI1 residues are in black. Location of K85 is labeled.



**Extended Data Fig. 2. Structural characterization of the RING1B-BMI1f interaction with RB-2.**  
**a** Superposition of the crystal structures of RING1B-BMI1f (colored gray) and RING1B-BMI1 complex (PDB 2CKL; RING1B is colored in magenta and BMI1 is blue). Positions of N- and C-termini are shown. **b** Crystal structure determined for RING1B-BMI1f co-crystallized with RB-2. Electron density is contoured at  $1\sigma$  (blue) and selected residues are labeled. **c** Crystal structure of RING1B-BMI1f co-crystallized with RB-2 shown in surface representation. Opened site exposing hydrophobic side chains of L80 and L100 (both in pale green) is shown. Surrounding positively charged residues are colored in pale blue. **d** Analysis of chemical shift perturbations determined for 120  $\mu\text{M}$  DCN RING1B-BMI1f upon binding with 500  $\mu\text{M}$  RB-2.  $\Delta_{\text{HN}}$  has been calculated as  $\sqrt{(\Delta\delta_{\text{HN}}^2 + 0.1 * \Delta\delta_{\text{N}}^2)}$  in ppm (top) and  $\Delta_{\text{CO}}$  is a difference in CO chemical shifts in ppm (bottom). **e** Strips from 3D  $^1\text{H}$ - $^{13}\text{C}$  HSQC-NOESY spectra for 290  $\mu\text{M}$  ILV  $^2\text{H}$ ,  $^{13}\text{C}$ ,  $^{15}\text{N}$  RING1B-BMI1f (black) and 120  $\mu\text{M}$  ILV  $^2\text{H}$ ,  $^{13}\text{C}$ ,  $^{15}\text{N}$  RING1B-BMI1f with 500  $\mu\text{M}$  RB-2 (blue). Assignment indicates NOEs

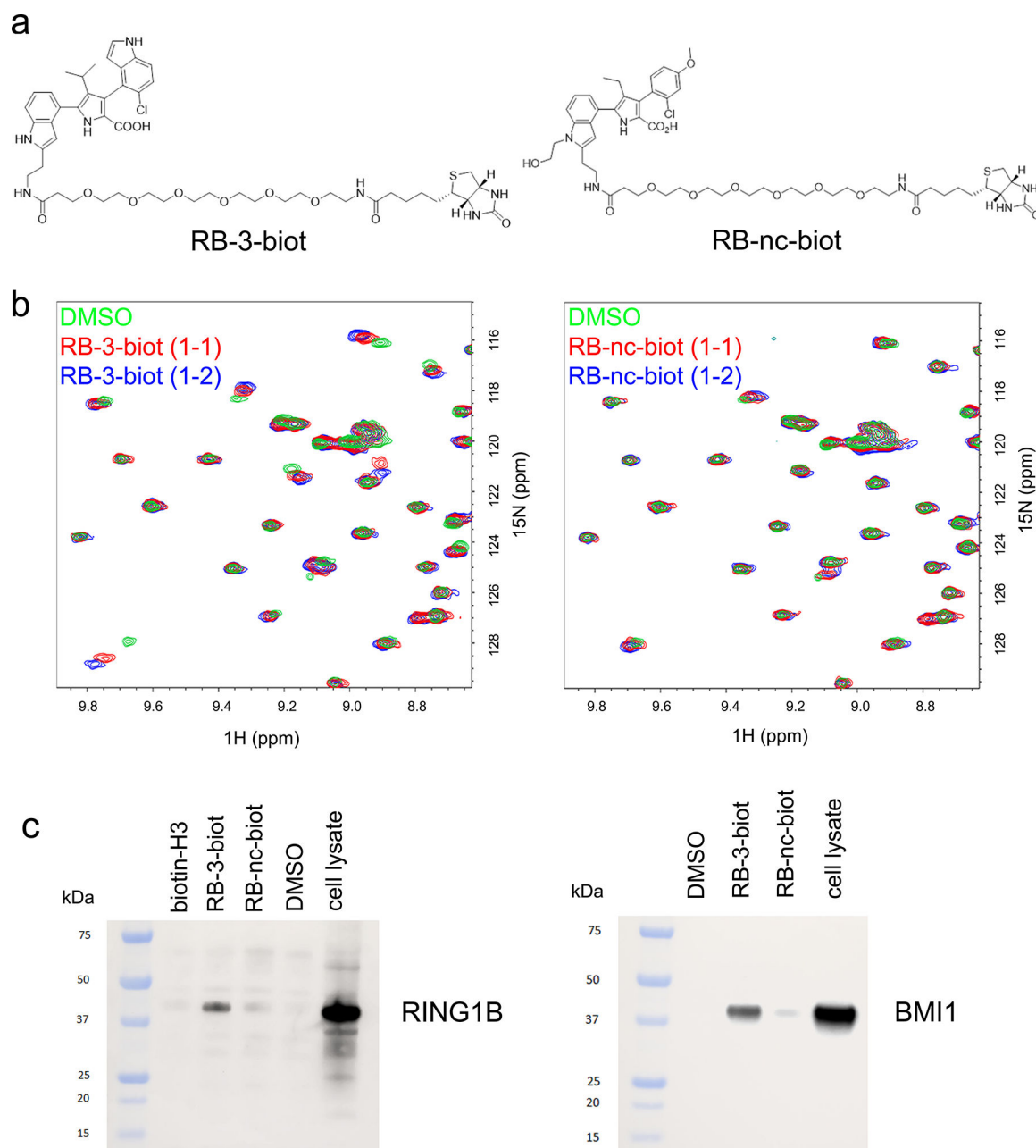
between RING1B-BMI1f protein and RB-2). **f**) Labeling of the RB-2 protons. **g**) 20 lowest energy conformers of RING1B-BMI1f with bound RB-2. RING1B residues are in pale green and BMI1 are in gray. RB-2 is shown with magenta carbons. **h**) Binding of RB-2 to the wild-type RING1B-BMI1 and RING1B(L94A)-BMI1f point mutant.  $^1\text{H}$ - $^{15}\text{N}$  HSQC spectra for  $60\ \mu\text{M}$   $^{15}\text{N}$  RING1B-BMI1f or  $60\ \mu\text{M}$   $^{15}\text{N}$  RING1B(L94A)-BMI1f (shown in red) are titrated with  $100\ \mu\text{M}$  RB-2 (shown in blue).



**Extended Data Fig. 3. Validation of the binding of RB-3 to RING1B-BMI1f and profiling the selectivity of RB-3.**

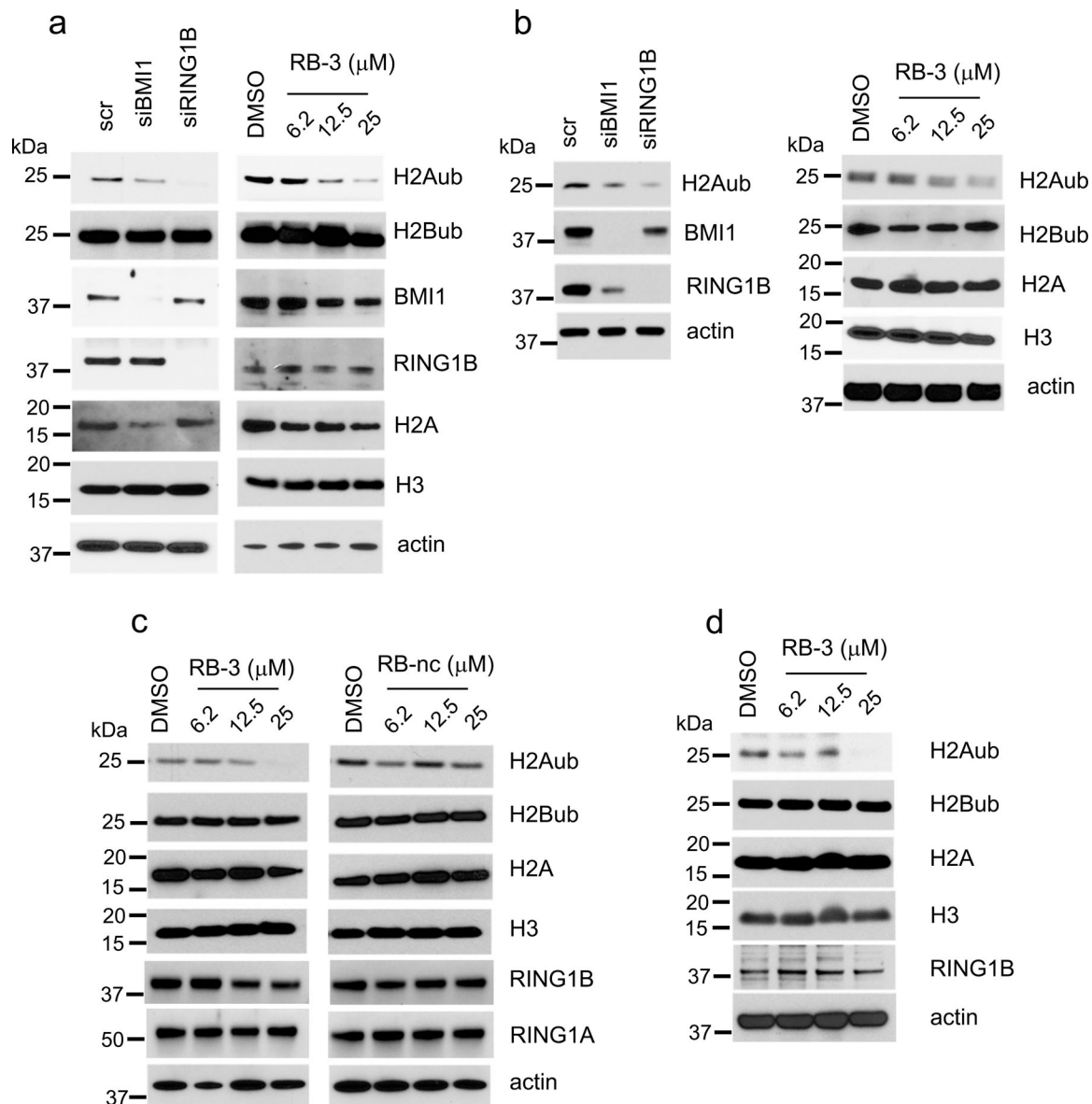
**a**) Assigned  $^1\text{H}$ - $^{13}\text{C}$  HSQC spectrum of  $60\ \mu\text{M}$   $^{13}\text{C}$ ,  $^{15}\text{N}$  RING1B-BMI1f (red) showing methyl group region superimposed onto the spectrum of  $60\ \mu\text{M}$   $^{13}\text{C}$ ,  $^{15}\text{N}$  RING1B-BMI1f with  $60\ \mu\text{M}$  RB-3 (blue). **b**) Comparison of the binding of RB-3 and RB-nc using NMR.  $^1\text{H}$ - $^{15}\text{N}$  HSQC spectra of  $60\ \mu\text{M}$   $^{15}\text{N}$  RING1B-BMI1f (red) titrated with  $100\ \mu\text{M}$  RB-nc (green),  $400\ \mu\text{M}$  RB-nc (blue) and  $100\ \mu\text{M}$  RB-3 (black). Of note,  $100\ \mu\text{M}$  RB-3 results in

almost complete saturation of chemical shift perturbations with 60  $\mu\text{M}$   $^{15}\text{N}$  RING1B-BMI1f. **c)** *In vitro* ubiquitination assay showing effect of RB-nc on RING1B-BMI1 E3 ligase activity. H2Aub was detected using Western blot and H3 was used as loading control. Lane with no E3 depicts sample without RING1B-BMI1f serving as negative control. Assay was repeated two times. **d)**  $^1\text{H}$ - $^{15}\text{N}$  HSQC spectrum of 60  $\mu\text{M}$   $^{15}\text{N}$  RING1B-BMI1f with 5% DMSO (black) superimposed onto 60  $\mu\text{M}$   $^{15}\text{N}$  RING1B-BMI1f with 60  $\mu\text{M}$  (blue) and 120  $\mu\text{M}$  RB-3 (red). **e)**  $^1\text{H}$ - $^{15}\text{N}$  HSQC spectrum of 60  $\mu\text{M}$   $^{15}\text{N}$  RING1A-BMI1f with 5% DMSO (black) superimposed onto 60  $\mu\text{M}$   $^{15}\text{N}$  RING1A-BMI1f with 60  $\mu\text{M}$  (blue) and 120  $\mu\text{M}$  RB-3 (red). **f)** *In vitro* ubiquitination assay showing the effect of RB-3 on RING1A-BMI1f and RING1B-BMI1f activity. H2Aub was detected using Western blot and H3 was used as loading control. Assays were repeated two times. **g)** *In vitro* ubiquitination assays showing no activity of RB-3 on BRCA1-BARD1, TRIM37 and RNF168. H2Aub is detected using Western blot and H3 or H2A was used as loading controls. Lanes with no E3 depicts samples without BRCA1-BARD1, TRIM37 or RNF168, respectively, serving as negative controls. Assays were repeated two times.



**Extended Data Fig. 4. Development and characterization of biotinylated RING1B probe compounds.**

a) structures of RB-3-biot and RB-nc-biot. b)  $^1\text{H}$ - $^{15}\text{N}$  HSQC spectra of  $60\ \mu\text{M}$   $^{15}\text{N}$  RING1B-BMI1f (green) titrated with  $60\ \mu\text{M}$  RB-3-biot or RB-nc-biot (red) and  $120\ \mu\text{M}$  RB-3-biot or RB-nc-biot (blue). c) Pull-down from HEK293T cells with RB-3-biot or RB-nc-biot followed by detection of RING1B or BMI1 using Western Blot analysis. Two controls were used in the pull-down assay, DMSO or biotinylated histone H3 peptide (biotin-H3), to assess non-specific binding. Assays were repeated two times



**Extended Data Fig. 5. RB-3 inhibits H2Aub in cancer cell lines.**

**a.** Evaluation of BMI1 and RING1B knockdown, and treatment with RB-3 in K562 cells.

*Left* western blot analysis in K562 cells transfected with BMI1/RING1B siRNAs for 96 h.

*Right* immunoblots of K562 cells treated with indicated doses of RB-3 for 96 hours.

Representative blots of two independent experiments are shown. **b.** Evaluation of BMI1 and

RING1B knockdown, and treatment with RB-3 in HeLa cells. *Left* Western blot in HeLa cells transfected with BMI1/RING1B siRNAs for 96 h. *Right* western blot analysis in HeLa

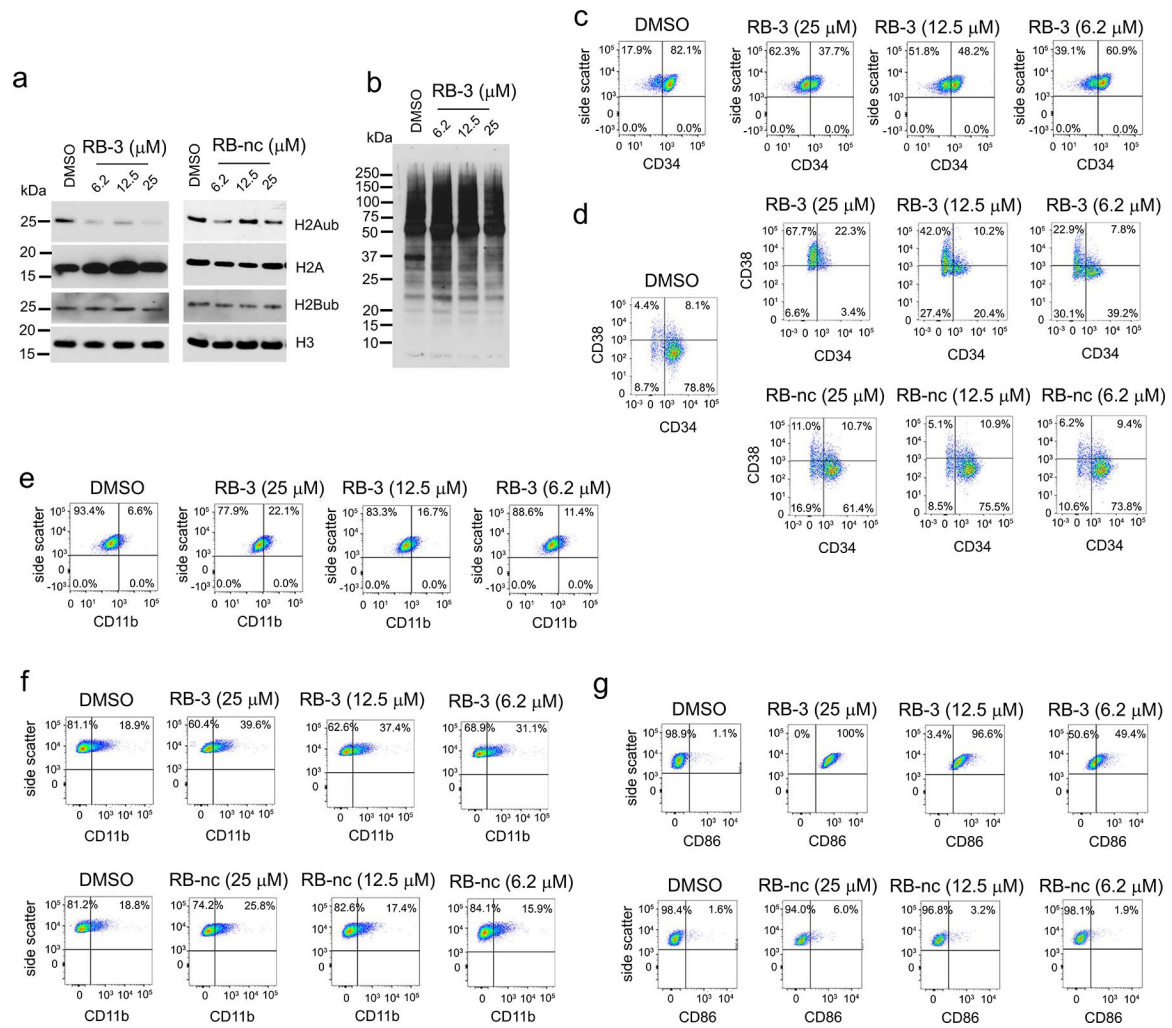
cells treated with indicated doses of RB-3 for 96 hours. Representative blots of two

independent experiments are shown. **c.** Activity of RB-3 and RB-nc in MOLM13 cells

treated for 96 hours with indicated doses of compounds. Representative blots of two

independent experiments are shown. **d.** Activity of RB-3 in MV4;11 cells treated for 96

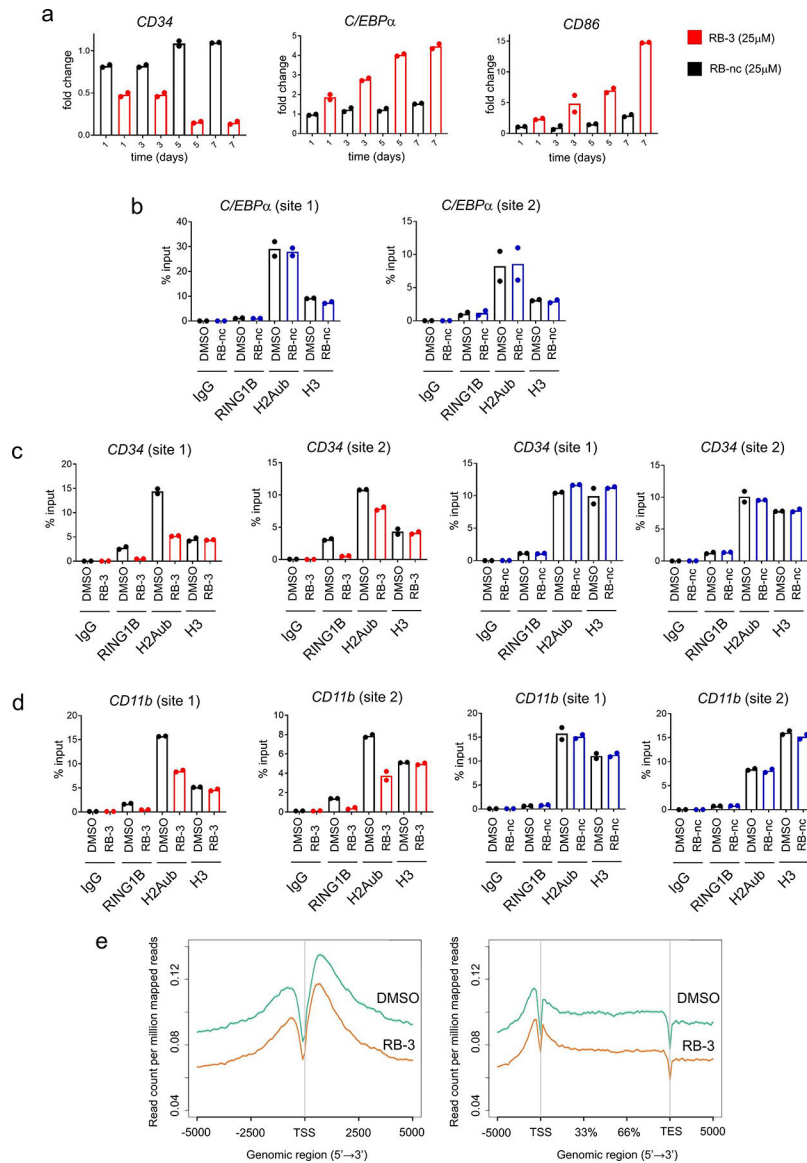
hours. Representative blots of two independent experiments are shown.



### Extended Data Fig. 6. Long-term effect of treatment of TEX cells with RB-3.

**a)** Western blot detection of H2Aub in TEX cells treated with increasing doses of RB-3 and RB-nc for 21 days. Representative blot out of two replicates. **b)** Western blot detection of total cellular ubiquitination levels using ubiquitin specific antibody in TEX cells treated with RB-3 for 21 days. Representative blot out of three replicates. **c)** Flow cytometry analysis of CD34 in TEX cells treated with RB-3 for 7 days. On day 7, cells were stained with APC/CY7-conjugated human anti-CD34 antibody and analyzed by FACS. Representative histograms of two independent experiments. **d)** Flow cytometry analysis of CD34 and CD38 in TEX cells treated with RB-3 (top panel) and RB-nc (bottom panel) for 21 days. On day 21, cells were stained with APC/CY7-conjugated human CD34 and PE-conjugated CD38 antibodies and analyzed by FACS. Representative histograms of two independent experiments. **e,f)** Flow cytometry analysis of myeloid differentiation marker CD11b/*ITGAM* in TEX cells treated with RB-3 for 7 days (**e**) and with RB-3 (**f**, top panel) and RB-nc (**f**, bottom panel) for 21 days. Cells were stained with Pacific Blue human CD11b antibody and analyzed by FACS. Representative histograms of two independent experiments. **g)** Flow cytometry analysis of dendritic cells differentiation marker CD86/B7-2 in TEX cells treated with RB-3 (top panel) and RB-nc (bottom panel) for 21 days. On day 21, cells were stained

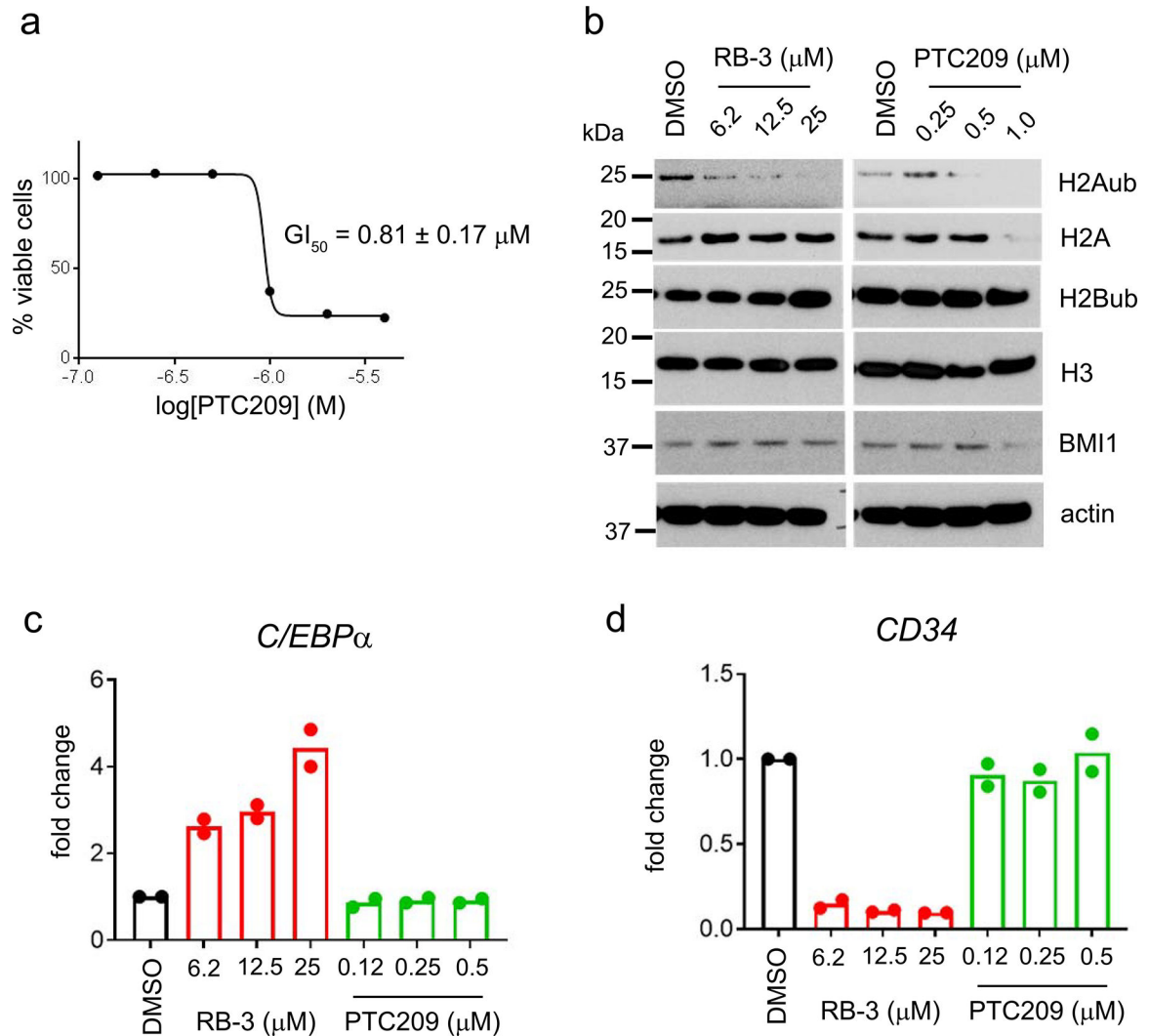
with Super Bight 436 conjugated human CD86 antibody and analyzed by FACS. Representative histograms of two independent experiments.



**Extended Data Fig. 7. RB-3 regulates expression of target genes and impairs enrichment of H2Aub and RING1B on target gene promoter regions in TEX cells.**

**a** qRT-PCR showing time dependent promoter changes in transcript levels of *CD34*, *C/EBPα*, *CD-86* upon treatment with 25 μM RB-3 and RB-nc. Representative data out of two replicates. **b**) Analysis of the H2Aub and H3 levels, and binding of RING1B to the two promoter regions of *C/EBPα* in TEX cells treated with RB-nc and DMSO for 8 days using ChIP assay. Representative data out of two replicates. **c**) Analysis of the H2Aub and H3 levels, and binding of RING1B to the two promoter regions of *CD34* in TEX cells treated with RB-3 (red), RB-nc (blue) and DMSO (black) for 8 days using ChIP assay. Representative data out of two replicates. **d**) Analysis of the H2Aub and H3 levels, and binding of RING1B to the two promoter regions of *CD11b* in TEX cells treated with RB-3 (red), RB-nc (blue) and

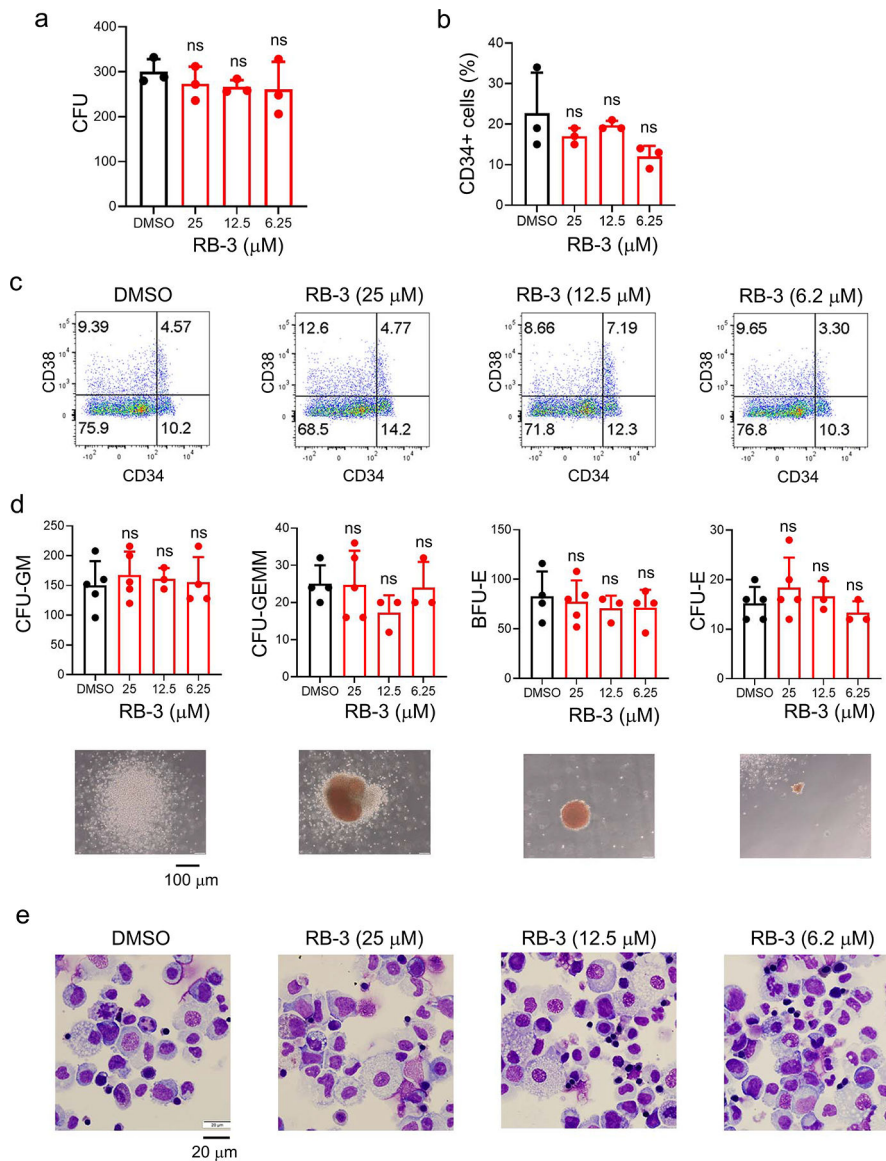
DMSO (black) for 8 days using ChIP assay. Representative data out of two replicates. Two promoter region primers between 1 to 2 kb upstream of the transcription start site (TSS) for each of *CD34*, *C/EBP $\alpha$*  and *CD11b* promoter were selected and analyzed (panels **b**, **c**, **d**). **e**) Average genome-wide occupancy of H2Aub around the transcription start sites (TSS) and genomic regions in TEX cells determined from ChIP-seq experiment. TEX cells were treated with DMSO and 25  $\mu$ M RB-3 for 6 days.



**Extended Data Fig. 8. Comparison of the activity of PTC209 and RB-3 in TEX cells.**

**a)** Graph showing effect of PTC209 on TEX cells proliferation. TEX cells were treated with the indicated concentrations of PTC209 for 4 days and processed for cell proliferation analysis. Experiment was performed 2 times,  $GI_{50}$  is mean  $\pm$  s.d. **b)** western blot showing levels of H2Aub, H2Bub, H2A, H3 and BMI1 in TEX cells treated for 4 days with indicated doses of RB-3 (left) and PTC209 (right). Representative blots from two independent experiments. **c)** qRT-PCR indicating levels of *C/EBP $\alpha$*  upon 96 hours treatment with indicated doses of RB-3 and PTC209. Representative data from two replicates. **d)** qRT-PCR

indicating levels of *CD34* upon 96 hours treatment with indicated doses of RB-3 and PTC209. Representative data from two replicates.



**Extended Data Fig. 9. RB-3 has no effect on normal CD34<sup>+</sup> cells.**

**a)** Quantitation of colony numbers (CFU) upon treatment of cord blood CD34<sup>+</sup> cells from healthy donors with RB-3. Experiments were performed two times and representative data are mean ± s.d. and analyzed by two-tailed t-test; ns – not significant. **b)** Population of CD34<sup>+</sup> cells upon treatment with RB-3. Experiments were performed two times and representative data are mean ± s.d. and analyzed by two-tailed t-test; ns – not significant. **c)** Flow-cytometry analysis of CD34 and CD38. Representative histograms of two independent experiments. **d)** Effect of RB-3 on various populations of mature cells with representative colony pictures. CFU-GM, granulocyte–macrophage progenitors; CFU-GEMM, oligopotential progenitors; BFU-E, burst-forming unit-erythroid cells; CFU-E, colony-

forming unit-erythroid cells. Experiments were performed two times and representative data are mean  $\pm$  s.d. and analyzed by two-tailed t-test; ns – not significant. e) Cell morphology of CD34<sup>+</sup> cells treated with RB-3 analyzed by Wright Giemsa staining. Representative slides are shown from two independent experiments.

## Supplementary Material

Refer to Web version on PubMed Central for supplementary material.

## Acknowledgements

This work was funded by the National Institute of Health (NIH) R01 grants CA207272, CA226759 and CA240514 to T.C. and CA201204, CA244254, CA160467 to J.G. and LLS Scholar grants (1340-17) to T.C. and (1215-14) to J.G. This research used resources of the Advanced Photon Source, a U.S. Department of Energy (DOE) Office of Science User Facility operated for the DOE Office of Science by Argonne National Laboratory under Contract No. DE-AC02-06CH11357. Use of the LS-CAT Sector 21 was supported by the Michigan Economic Development Corporation and the Michigan Technology Tri-Corridor (Grant 085P1000817). TEX and MLL-ENL cells have been received from Dr J. Dick, University Health Network, Toronto, Canada. We thank Dr. Martin Carroll and Dr. Gwenn Danet-Desnoyers from Stem Cell and Xenograft Core at the University of Pennsylvania for providing a patient sample.

## References

1. Simon JA & Kingston RE Mechanisms of polycomb gene silencing: knowns and unknowns. *Nat Rev Mol Cell Biol* 10, 697–708 (2009). [PubMed: 19738629]
2. Chittock EC, Latwiel S, Miller TC & Muller CW Molecular architecture of polycomb repressive complexes. *Biochem Soc Trans* 45, 193–205 (2017). [PubMed: 28202673]
3. Gao Z et al. PCGF homologs, CBX proteins, and RYBP define functionally distinct PRC1 family complexes. *Mol Cell* 45, 344–56 (2012). [PubMed: 22325352]
4. Taherbhoy AM, Huang OW & Cochran AG BMI1-RING1B is an autoinhibited RING E3 ubiquitin ligase. *Nat Commun* 6, 7621 (2015). [PubMed: 26151332]
5. Scelfo A et al. Functional Landscape of PCGF Proteins Reveals Both RING1A/B-Dependent-and RING1A/B-Independent-Specific Activities. *Mol Cell* 74, 1037–1052 e7 (2019). [PubMed: 31029542]
6. Buchwald G et al. Structure and E3-ligase activity of the Ring-Ring complex of polycomb proteins Bmi1 and Ring1b. *EMBO J* 25, 2465–74 (2006). [PubMed: 16710298]
7. Tamburri S et al. Histone H2AK119 Mono-Ubiquitination Is Essential for Polycomb-Mediated Transcriptional Repression. *Mol Cell* 77, 840–856 e5 (2020). [PubMed: 31883952]
8. Blackledge NP et al. PRC1 Catalytic Activity Is Central to Polycomb System Function. *Mol Cell* 77, 857–874 e9 (2020). [PubMed: 31883950]
9. McGinty RK, Henrici RC & Tan S Crystal structure of the PRC1 ubiquitylation module bound to the nucleosome. *Nature* 514, 591–6 (2014). [PubMed: 25355358]
10. Blackledge NP et al. Variant PRC1 complex-dependent H2A ubiquitylation drives PRC2 recruitment and polycomb domain formation. *Cell* 157, 1445–1459 (2014). [PubMed: 24856970]
11. Rose NR et al. RYBP stimulates PRC1 to shape chromatin-based communication between Polycomb repressive complexes. *Elife* 5(2016).
12. Fursova NA et al. Synergy between Variant PRC1 Complexes Defines Polycomb-Mediated Gene Repression. *Mol Cell* 74, 1020–1036 e8 (2019). [PubMed: 31029541]
13. Bonnet D & Dick JE Human acute myeloid leukemia is organized as a hierarchy that originates from a primitive hematopoietic cell. *Nat Med* 3, 730–7 (1997). [PubMed: 9212098]
14. Kreso A et al. Self-renewal as a therapeutic target in human colorectal cancer. *Nat Med* 20, 29–36 (2014). [PubMed: 24292392]
15. Martin-Perez D, Piris MA & Sanchez-Beato M Polycomb proteins in hematologic malignancies. *Blood* 116, 5465–75 (2010). [PubMed: 20716771]

16. Sauvageau M & Sauvageau G Polycomb group proteins: multi-faceted regulators of somatic stem cells and cancer. *Cell Stem Cell* 7, 299–313 (2010). [PubMed: 20804967]
17. Lessard J & Sauvageau G Bmi-1 determines the proliferative capacity of normal and leukaemic stem cells. *Nature* 423, 255–60 (2003). [PubMed: 12714970]
18. Shima H et al. Ring1A and Ring1B inhibit expression of Glis2 to maintain murine MOZ-TIF2 AML stem cells. *Blood* 131, 1833–1845 (2018). [PubMed: 29371181]
19. Rizo A et al. Repression of BMI1 in normal and leukemic human CD34(+) cells impairs self-renewal and induces apoptosis. *Blood* 114, 1498–505 (2009). [PubMed: 19556423]
20. van den Boom V et al. Non-canonical PRC1.1 Targets Active Genes Independent of H3K27me3 and Is Essential for Leukemogenesis. *Cell Rep* 14, 332–46 (2016). [PubMed: 26748712]
21. Alchanati I et al. The E3 ubiquitin-ligase Bmi1/Ring1A controls the proteasomal degradation of Top2alpha cleavage complex - a potentially new drug target. *PLoS One* 4, e8104 (2009). [PubMed: 19956605]
22. Su W et al. The Polycomb Repressor Complex 1 Drives Double-Negative Prostate Cancer Metastasis by Coordinating Stemness and Immune Suppression. *Cancer Cell* 36, 139–155 e10 (2019). [PubMed: 31327655]
23. Li Z et al. Structure of a Bmi-1-Ring1B polycomb group ubiquitin ligase complex. *J Biol Chem* 281, 20643–9 (2006). [PubMed: 16714294]
24. van Zundert GCP et al. The HADDOCK2.2 Web Server: User-Friendly Integrative Modeling of Biomolecular Complexes. *J Mol Biol* 428, 720–725 (2016). [PubMed: 26410586]
25. Bhatnagar S et al. TRIM37 is a new histone H2A ubiquitin ligase and breast cancer oncoprotein. *Nature* 516, 116–20 (2014). [PubMed: 25470042]
26. Kalb R, Mallery DL, Larkin C, Huang JT & Hiom K BRCA1 is a histone-H2A-specific ubiquitin ligase. *Cell Rep* 8, 999–1005 (2014). [PubMed: 25131202]
27. Horn V et al. Structural basis of specific H2A K13/K15 ubiquitination by RNF168. *Nat Commun* 10, 1751 (2019). [PubMed: 30988309]
28. Dixon AS et al. NanoLuc Complementation Reporter Optimized for Accurate Measurement of Protein Interactions in Cells. *ACS Chem Biol* 11, 400–8 (2016). [PubMed: 26569370]
29. Warner JK et al. Direct evidence for cooperating genetic events in the leukemic transformation of normal human hematopoietic cells. *Leukemia* 19, 1794–805 (2005). [PubMed: 16094415]
30. McDermott SP et al. A small molecule screening strategy with validation on human leukemia stem cells uncovers the therapeutic efficacy of kinetin riboside. *Blood* 119, 1200–7 (2012). [PubMed: 22160482]
31. van Rhenen A et al. High stem cell frequency in acute myeloid leukemia at diagnosis predicts high minimal residual disease and poor survival. *Clin Cancer Res* 11, 6520–7 (2005). [PubMed: 16166428]
32. Pulikkan JA, Tenen DG & Behre G C/EBPalpha deregulation as a paradigm for leukemogenesis. *Leukemia* 31, 2279–2285 (2017). [PubMed: 28720765]
33. Yu M et al. Direct recruitment of polycomb repressive complex 1 to chromatin by core binding transcription factors. *Mol Cell* 45, 330–43 (2012). [PubMed: 22325351]
34. Barbour H, Daou S, Hendzel M & Affar EB Polycomb group-mediated histone H2A monoubiquitination in epigenome regulation and nuclear processes. *Nat Commun* 11, 5947 (2020). [PubMed: 33230107]
35. Cales C et al. Inactivation of the polycomb group protein Ring1B unveils an antiproliferative role in hematopoietic cell expansion and cooperation with tumorigenesis associated with Ink4a deletion. *Mol Cell Biol* 28, 1018–28 (2008). [PubMed: 18039844]
36. Nishida Y et al. Preclinical activity of the novel B-cell-specific Moloney murine leukemia virus integration site 1 inhibitor PTC-209 in acute myeloid leukemia: Implications for leukemia therapy. *Cancer Sci* 106, 1705–13 (2015). [PubMed: 26450753]
37. Barabe F, Kennedy JA, Hope KJ & Dick JE Modeling the initiation and progression of human acute leukemia in mice. *Science* 316, 600–4 (2007). [PubMed: 17463288]
38. Jeusset LM & McManus KJ Developing Targeted Therapies That Exploit Aberrant Histone Ubiquitination in Cancer. *Cells* 8(2019).

39. Park IK et al. Bmi-1 is required for maintenance of adult self-renewing haematopoietic stem cells. *Nature* 423, 302–5 (2003). [PubMed: 12714971]
40. Su WJ et al. RNF2/Ring1b negatively regulates p53 expression in selective cancer cell types to promote tumor development. *Proc Natl Acad Sci U S A* 110, 1720–5 (2013). [PubMed: 23319651]
41. Ardley HC Ring finger ubiquitin protein ligases and their implication to the pathogenesis of human diseases. *Curr Pharm Des* 15, 3697–715 (2009). [PubMed: 19925421]
42. Duffy MJ, Synnott NC, O’Grady S & Crown J Targeting p53 for the treatment of cancer. *Semin Cancer Biol* (2020).
43. Watt GF, Scott-Stevens P & Gaohua L Targeted protein degradation in vivo with Proteolysis Targeting Chimeras: Current status and future considerations. *Drug Discov Today Technol* 31, 69–80 (2019). [PubMed: 31200862]
44. Gray F et al. BMI1 regulates PRC1 architecture and activity through homo- and hetero-oligomerization. *Nat Commun* 7, 13343 (2016). [PubMed: 27827373]
45. Jaatinen T et al. Global gene expression profile of human cord blood-derived CD133+ cells. *Stem Cells* 24, 631–41 (2006). [PubMed: 16210406]
46. Gal H et al. Gene expression profiles of AML derived stem cells; similarity to hematopoietic stem cells. *Leukemia* 20, 2147–54 (2006). [PubMed: 17039238]
47. Sheffield PJ, Derewenda U, Taylor J, Parsons TJ & Derewenda ZS Expression, purification and crystallization of a BH domain from the GTPase regulatory protein associated with focal adhesion kinase. *Acta Crystallogr D Biol Crystallogr* 55, 356–9 (1999). [PubMed: 10232922]
48. Brzovic PS et al. Binding and recognition in the assembly of an active BRCA1/BARD1 ubiquitin-ligase complex. *Proc Natl Acad Sci U S A* 100, 5646–51 (2003). [PubMed: 12732733]
49. Wiener R et al. E2 ubiquitin-conjugating enzymes regulate the deubiquitinating activity of OTUB1. *Nat Struct Mol Biol* 20, 1033–9 (2013). [PubMed: 23955022]
50. Delaglio F et al. NMRPipe: a multidimensional spectral processing system based on UNIX pipes. *J Biomol NMR* 6, 277–93 (1995). [PubMed: 8520220]
51. Tugarinov V & Kay LE Quantitative NMR studies of high molecular weight proteins: application to domain orientation and ligand binding in the 723 residue enzyme malate synthase G. *J Mol Biol* 327, 1121–33 (2003). [PubMed: 12662935]
52. Otwinowski Z & Minor W Processing of X-ray diffraction data collected in oscillation mode. *Methods Enzymol* 276, 307–26 (1997).
53. Vagin A & Teplyakov A Molecular replacement with MOLREP. *Acta Crystallogr D Biol Crystallogr* 66, 22–5 (2010). [PubMed: 20057045]
54. Emsley P, Lohkamp B, Scott WG & Cowtan K Features and development of Coot. *Acta Crystallogr D Biol Crystallogr* 66, 486–501 (2010). [PubMed: 20383002]
55. Afonine PV et al. Towards automated crystallographic structure refinement with phenix.refine. *Acta Crystallogr D Biol Crystallogr* 68, 352–67 (2012). [PubMed: 22505256]
56. McCoy AJ et al. Phaser crystallographic software. *J Appl Crystallogr* 40, 658–674 (2007). [PubMed: 19461840]
57. Tugarinov V & Kay LE Ile, Leu, and Val methyl assignments of the 723-residue malate synthase G using a new labeling strategy and novel NMR methods. *J Am Chem Soc* 125, 13868–78 (2003). [PubMed: 14599227]
58. Huang H et al. Covalent inhibition of NSD1 histone methyltransferase. *Nat Chem Biol* 16, 1403–1410 (2020). [PubMed: 32868895]
59. Egan B et al. An Alternative Approach to ChIP-Seq Normalization Enables Detection of Genome-Wide Changes in Histone H3 Lysine 27 Trimethylation upon EZH2 Inhibition. *PLoS One* 11, e0166438 (2016). [PubMed: 27875550]
60. Grembecka J et al. Menin-MLL inhibitors reverse oncogenic activity of MLL fusion proteins in leukemia. *Nat Chem Biol* 8, 277–84 (2012). [PubMed: 22286128]

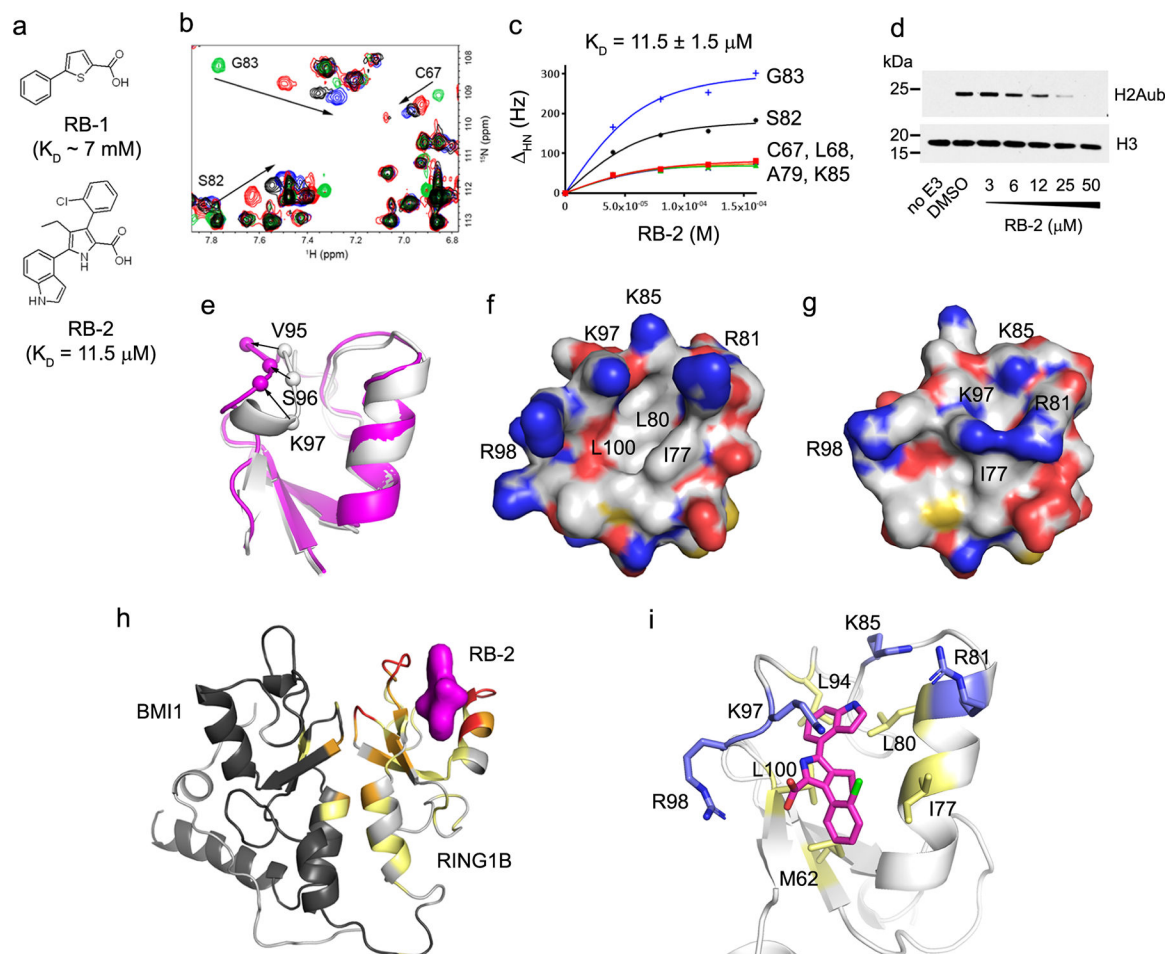


**Figure 1. Development and structural characterization of PRC1 inhibitor RB-2.**

**a**, Structures and activities of fragment hit RB-1 and optimized analog RB-2. **b**, Superposition of the  $^1\text{H}$ - $^{15}\text{N}$  HSQC spectra of 60  $\mu\text{M}$  RING1B-BMI1f with 5% DMSO (green) titrated with 40  $\mu\text{M}$  (red), 80  $\mu\text{M}$  (black) and 160  $\mu\text{M}$  (blue) RB-2. **c**, Determination of  $K_D$  for RB-2 binding to RING1B-BMI1f using NMR.  $K_D$  is mean  $\pm$  s.d. calculated from titration of six different amides. **d**, Inhibition of RING1B-BMI1f E3 ligase activity with RB-2 using *in vitro* ubiquitination assay. Assay was repeated 3 times. **e**, Superposition of the crystal structures of RING1B-BMI1f in free form (closed, shown in white) and co-crystallized with RB-2 (open, shown in magenta). Fragment of the RING domain of RING1B is shown with positions of CA atoms of selected residues experiencing the largest conformational changes. **f**, **g**, Crystal structures of RING1B-BMI1f showing RING domains of RING1B in open (**f**) and closed (**g**) conformations. Protein is shown in surface representation in the same orientation as in panel **e**. **h**, Structural model of RING1B-BMI1f (shown in ribbon) with bound RB-2 (shown in surface representation in magenta) determined using joint refinement based on X-ray crystallography and NMR data. Protein is colored according to the magnitude of chemical shift perturbations ( $\Delta_{\text{HN}}$ ) determined from NMR for 120  $\mu\text{M}$  RING1B-BMI1f without and with 500  $\mu\text{M}$  RB-2:  $\Delta_{\text{HN}} < 0.03$  (gray);  $0.03 < \Delta_{\text{HN}} < 0.09$  (yellow);  $0.09 < \Delta_{\text{HN}} < 0.2$  (orange);  $\Delta_{\text{HN}} > 0.2$  (red); unassigned residues are in white. **i**, Details of RB-2 binding site on RING1B. RB-2 is shown with magenta carbons

and selected protein residues are in sticks colored in yellow (hydrophobic residues) or blue (positively charged residues).

Author Manuscript

Author Manuscript

Author Manuscript

Author Manuscript

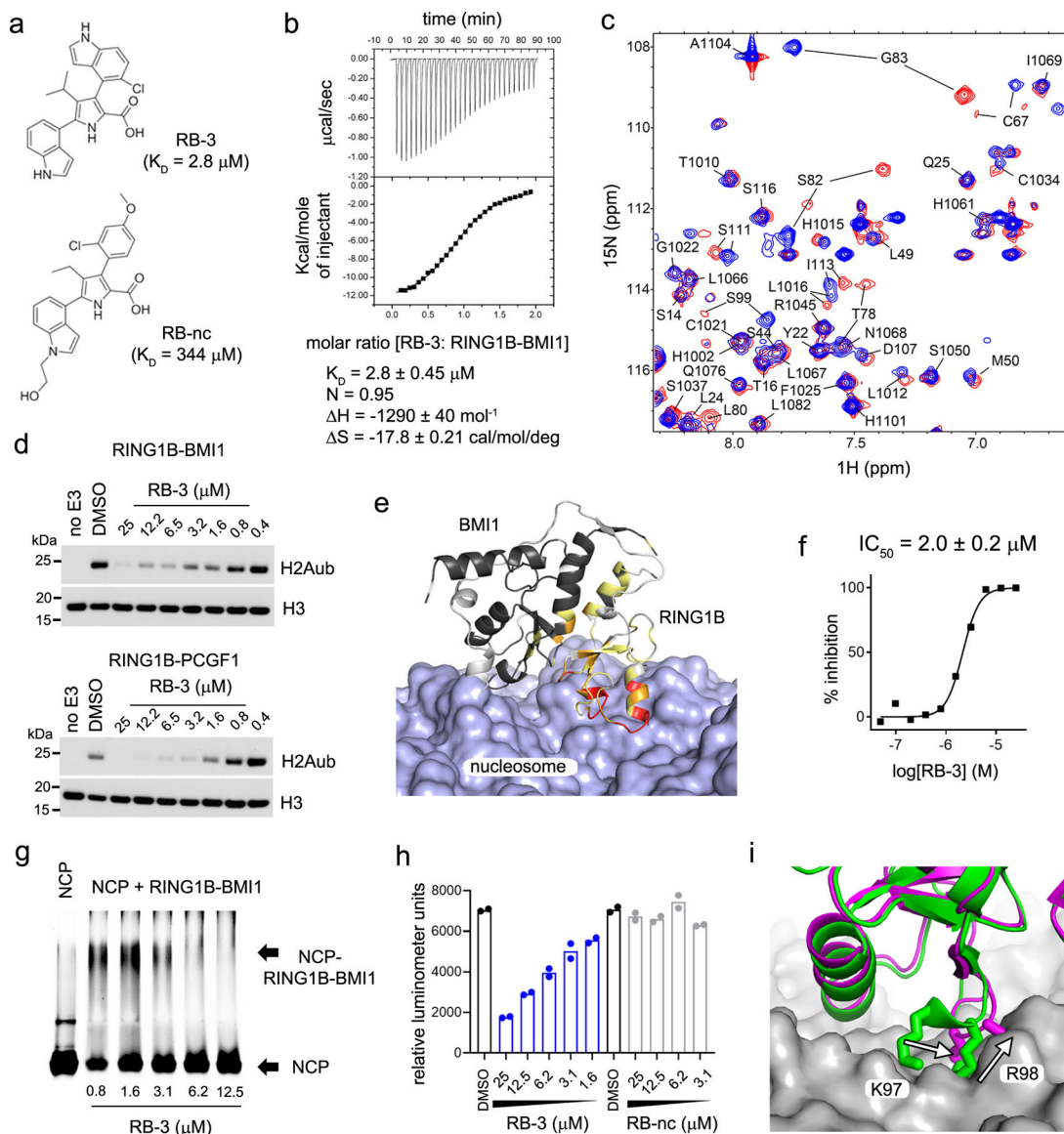


**Figure 2. RB-3 inhibits PRC1 and disrupts the interaction with nucleosomes.**  
**a.** Structures and activities of RB-3 and RB-nc. Binding affinities determined by ITC (RB-3) and NMR (RB-nc). **b.** Characterization of the binding of RB-3 to RING1B-BMI1f using ITC. Data are mean  $\pm$  s.d. from two independent experiments. **c.** Fragment of  $^1\text{H}$ - $^{15}\text{N}$  HSQC spectrum of 250  $\mu\text{M}$  RING1B-BMI1f without (blue) and with 500  $\mu\text{M}$  RB-3 (red). Assignment shows chemical shift perturbations upon binding of RB-3 to RING1B-BMI1f. **d.** *In vitro* ubiquitination assay showing the inhibition of heterodimeric RING1B-BMI1 and RING1B-PCGF1 by RB-3. Representative blots of two independent experiments. **e.** Analysis of chemical shift perturbations  $^1\text{H}_\text{N}$  (ppm) determined upon binding of 120  $\mu\text{M}$  RING1B-BMI1f with 500  $\mu\text{M}$  RB-2 mapped on the crystal structure of RING1B-BMI1 bound to nucleosome (PDB 4R8P). Residues are colored as follows:  $^1\text{H}_\text{N} < 0.03$  (gray);  $0.03 < ^1\text{H}_\text{N} < 0.09$  (yellow);  $0.09 < ^1\text{H}_\text{N} < 0.2$  (orange);  $^1\text{H}_\text{N} > 0.2$  (red). **f.** RB-3 blocks interaction between RING1B-BMI1f and biotinylated nucleosomes determined using

AlphaScreen assay. Data are mean  $\pm$  s.d. from two independent experiments. **g**, EMSA assay showing activity of RB-3 to disrupt RING1B-BMI1f binding to recombinant nucleosomes (NCP). Bands corresponding to NCP and RING1B-BMI1-NCP complex are labeled. Representative image of two independent experiments. **h**, Inhibition of RING1B interaction with chromatin in HEK293T cells determined using NanoBiT assay. Representative data of two independent experiments. **i**, Superposition of the crystal structure of RING1B-BMI1f determined in the presence of RB-2 (magenta) onto the structure of RING1B-BMI1 bound to nucleosome (green, PDB 4R8P). Nucleosome is shown as gray surface and arrows highlight conformational change in RING1B side chains upon ligand binding.

Author Manuscript

Author Manuscript

Author Manuscript

Author Manuscript

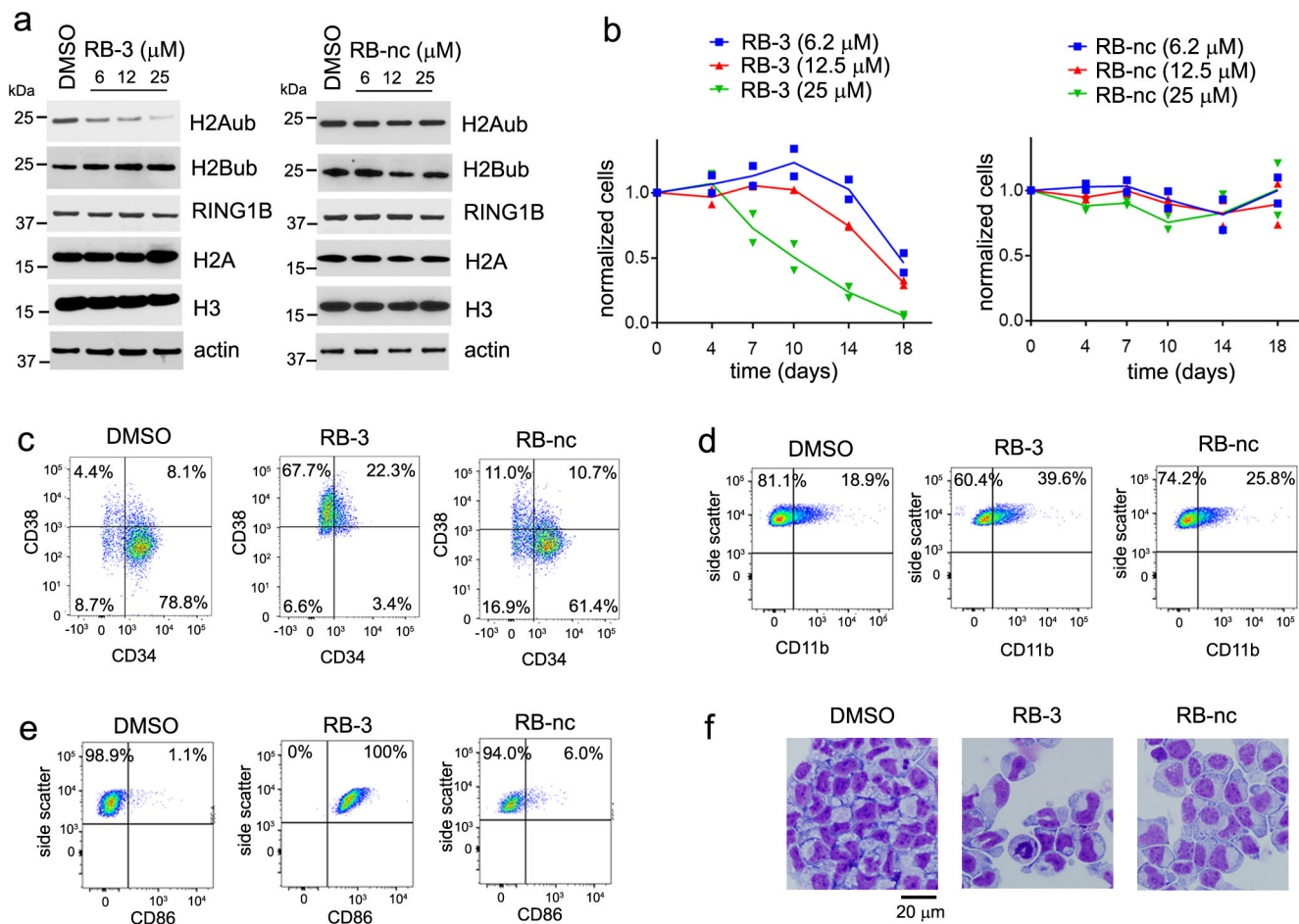


**Figure 3. Treatment with RB-3 leads to reduction in H2Aub and differentiation in TEX cells.**

**a**, Assessment of H2Aub, H2Bub, H3 and total H2A in TEX cells treated with RB-3 (left) or RB-nc (right) for 4 days. Representative gel of three independent experiments. **b**, Effect of RING1B inhibition on the growth of TEX cells treated with RB-3 and RB-nc. Representative data from two independent experiments. **c**, **d**, **e**, Flow-cytometry analysis of CD34 and CD38 (**c**), CD11b (**d**) and CD86 (**e**) expression in TEX cells treated with 25 μM RB-3 and 25 μM RB-nc for 21 days. Representative histograms of two independent experiments. **f**, Cell morphology of TEX cells after 21 days of treatment with 25 μM RB-3, 25 μM RB-nc or DMSO analyzed by Wright Giemsa staining. Representative slides are shown from two independent experiments.

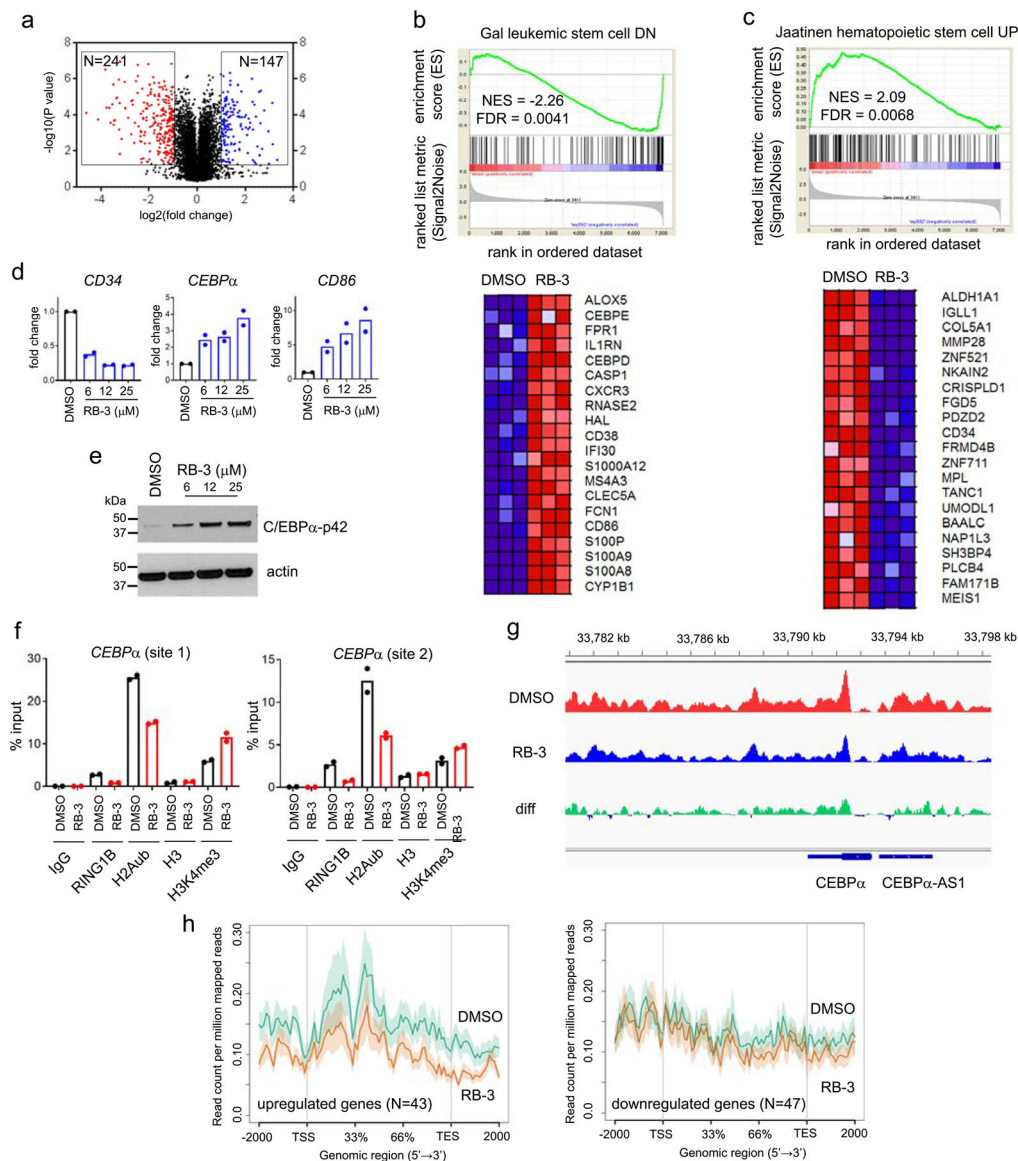


**Figure 4. RB-3 reduces H2Aub via disruption of PRC1 binding to target genes.**

**a**, Volcano plot showing changes in gene expression upon treatment of TEX cells with 25  $\mu$ M RB-3 for 6 days. Triplicate samples were used for global gene expression studies. **b**, **c**, Gene set enrichment analysis (GSEA) of genes upregulated (**b**) and downregulated (**c**) upon treatment with RB-3 or DMSO in TEX cells for 6 days using gene sets defined by Jaatinen et al.<sup>45</sup> and Gal et al.<sup>46</sup>. The heatmaps show genes comprising the leading edge of the GSEA plots. Red, high expression; blue, low expression. **d**, qPCR analysis of *CD34*, *CD86* and *C/EBP $\alpha$*  expression levels in TEX cells treated with RB-3 for 8 days. Representative data from two independent experiments. **e**, Western blot of C/EBP $\alpha$  in TEX cells treated with RB-3 for 8 days. Representative data from three independent experiments. **f**, ChIP-qPCR analysis of H2Aub, RING1B, H3 and H3K4me3 occupancy at two sites within the promoter of C/EBP $\alpha$  in TEX cells treated with DMSO or 25  $\mu$ M RB-3 for 8 days. Representative data from two independent experiments. **g**, Genome browser view of H2Aub occupancy across the C/

EBP $\alpha$  locus. Normalized ChIP-seq signal is shown for TEX cells treated with DMSO (red), RB-3 (blue) and difference (green). **h**, Meta-gene profiles for spike-in normalized H2Aub ChIP-Seq signal over genomic regions corresponding to the most upregulated and downregulated genes in TEX cells treated with DMSO and 25 $\mu$ M RB-3 for 6 days. TSS – transcription start site; TES – transcription end site.

Author Manuscript

Author Manuscript

Author Manuscript

Author Manuscript

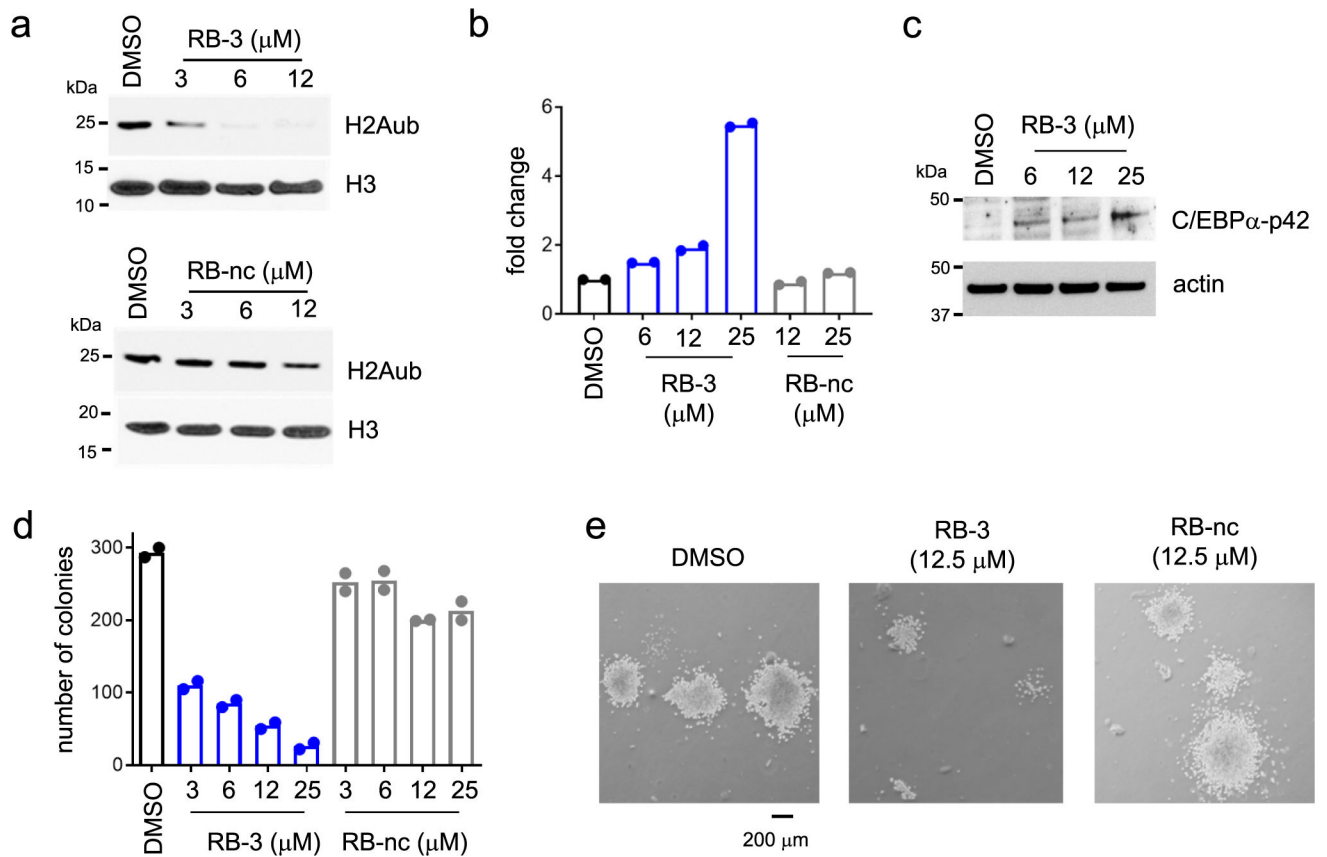


**Figure 5. Treatment with RB-3 reduces colony forming capacity of MLL-ENL cells.**

**a**, Western blot detection of H2Aub, and H3 in MLL-ENL cells obtained from colony assay treated with increasing doses of RB-3 and RB-nc for 7 days. Representative data from two independent experiments. **b**, Expression of C/EBP $\alpha$  measured by qRT-PCR in MLL-ENL cells treated with RB-3 and RB-nc for 8 days. Transcript levels are normalized to GAPDH. Representative data are from two independent experiments. **c**, Analysis of C/EBP $\alpha$ -p42 levels in MLL-ENL cells treated with RB-3 for 8 days. Representative blot from two independent experiments. **d**, Colony assay performed in MLL-ENL cells treated for 14 days with RB-3 and RB-nc. Representative data from two independent experiments. **e**, Colonies in MLL-ENL cells after treatment with RB-3 and RB-nc for 14 days. Representative pictures from two independent experiments.

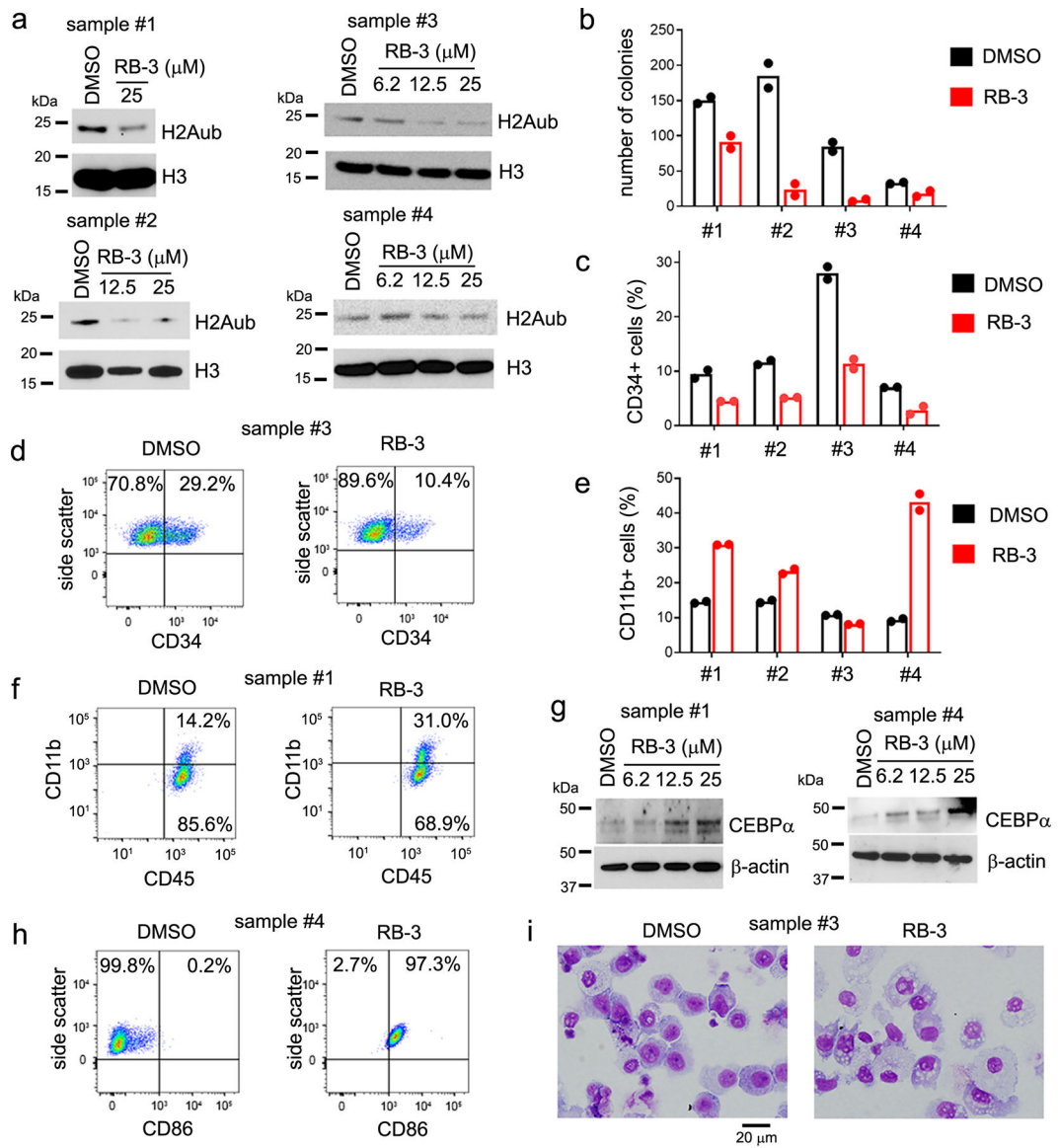


**Figure 6. RB-3 reduces global H2Aub levels and induces differentiation in primary AML patient samples.**

**a**, Western blot detection of H2Aub, and H3 in four primary AML patient samples treated with RB-3 for 12 days. Western blots were performed once due to limited amounts of primary samples. **b**, Colony counts from the second round of colony forming assay in primary AML patient samples treated with 25  $\mu$ M RB-3 for 14 days. Data are two technical replicates from single experiment. **c**, Quantification of CD34<sup>+</sup> cells in primary AML patient samples treated with 25  $\mu$ M RB-3 for 12 days. Data are two technical replicates from single experiment. **d**, Representative FACS histograms showing the level of CD34<sup>+</sup> cells for sample #3 treated with 25  $\mu$ M RB-3 and 25  $\mu$ M RB-nc for 12 days. **e**, Flow cytometry quantitation of CD11b<sup>+</sup> cells in primary AML samples treated with 25  $\mu$ M RB-3 for 12 days. Data are two technical replicates from single experiment. **f**, Representative FACS histograms showing the level of CD11b<sup>+</sup> cells for sample #1 treated with 25  $\mu$ M RB-3 and 25  $\mu$ M RB-nc. **g**, Western blot detection of C/EBP $\alpha$ -p42 and  $\beta$ -actin levels in AML samples

treated with RB-3 for 12 days. Western blots were performed once. **h**, Representative FACS histograms showing CD86 level in sample #4 treated with 25  $\mu$ M RB-3 and 25  $\mu$ M RB-nc for 12 days. **i**, Cell morphology of AML cells analyzed by Wright-Giemsa Giemsa staining after 14 days treatment with 25  $\mu$ M RB-3 or DMSO. Representative slides from single experiment.

Author Manuscript

Author Manuscript

Author Manuscript

Author Manuscript